JCTC Journal of Chemical Theory and Computation

Article

pubs.acs.org/JCTC

CC/DFT Route toward Accurate Structures and Spectroscopic Features for Observed and Elusive Conformers of Flexible Molecules: Pyruvic Acid as a Case Study

Vincenzo Barone,*[,†] Malgorzata Biczysko,[‡] Julien Bloino,[‡] Paola Cimino,[¶] Emanuele Penocchio,[†] and Cristina Puzzarini[§]

[†]Scuola Normale Superiore, Piazza dei Cavalieri 7, I-56126 Pisa, Pisa, Italy

[‡]Consiglio Nazionale delle Ricerche, Istituto di Chimica dei Composti OrganoMetallici (ICCOM-CNR), UOS di Pisa, Area della Ricerca CNR, Via G. Moruzzi 1, I-56124 Pisa, Pisa, Italy

[¶]Dipartimento di Scienze Farmaceutiche, Università degli Studi di Salerno, via Ponte don Melillo, I-84084 Fisciano, Salerno, Italy

[§]Dipartimento di Chimica "Giacomo Ciamician", Università di Bologna, Via Selmi 2, I-40126 Bologna, Bologna, Italy

Supporting Information

ABSTRACT: The structures and relative stabilities as well as the rotational and vibrational spectra of the three low-energy conformers of pyruvic acid (PA) have been characterized using a state-of-the-art quantum-mechanical approach designed for flexible molecules. By making use of the available experimental rotational constants for several isotopologues of the most stable PA conformer, *Tc*-PA, the semiexperimental equilibrium structure has been derived. The latter provides a reference for the pure theoretical determination of the equilibrium geometries for all conformers, thus confirming for these structures an accuracy of 0.001 Å and 0.1 deg for bond lengths and angles, respectively. Highly accurate relative energies of all conformers (*Tc*-, *Tt*-, and *Ct*-PA) and of the transition states connecting them are provided along with the thermodynamic properties at low and high temperatures, thus leading to conformational enthalpies accurate to 1 kJ mol^{-1}. Concerning microwave spectroscopy, rotational constants accurate to about 20 MHz are provided for the *Tt*- and *Ct*-PA conformers, together with the computed centrifugal-distortion constants and dipole moments required to simulate their rotational spectra. For *Ct*-PA, vibrational frequencies in the mid-infrared region accurate to 10 cm^{-1} are reported along with theoretical estimates for the transitions in the near-infrared range, and the corresponding infrared spectrum including fundamental transitions, overtones, and combination bands has been simulated. In addition to the new data described above, theoretical results for the *Tc*- and *Tt*-PA conformers are compared with all available experimental data to further confirm the accuracy of the hybrid coupled-cluster/density functional theory (CC/DFT) protocol applied in the present study. Finally, we discuss in detail the accuracy of computational models fully based on double-hybrid DFT functionals (mainly at the B2PLYP/aug-cc-pVTZ level) that avoid the use of very expensive CC calculations.

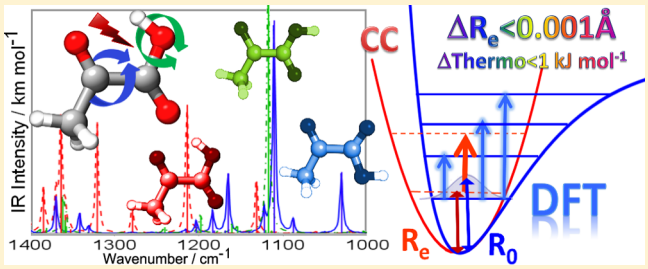

1. INTRODUCTION

There is an increasing interest in detailed knowledge of the conformational behavior of the main building blocks of biomolecules (amino acids, nucleic bases, carbohydrates, etc.) without the perturbing effect of the environment (unavoidable in condensed phases).[1−10] Indeed, this is a mandatory prerequisite toward the understanding of the role played by different interactions in determining the biological activity in terms of structure−activity relationships. In particular, a great effort has been carried out for the determination of molecular structures and properties of biomolecule building blocks of increasing size and complexity[11−18] as well as of less-stable conformers of well-known small- to medium-sized organic molecules containing the typical bond patterns of biomolecular systems.[19−29] For the latter, several attempts have recently been performed in order to either detect less stable conformers in the experimental mixtures or to generate new ones by suitable spectroscopic experiments. In all these cases, the accurate theoretical characterization of molecular structures, rotational and vibrational properties, and in particular the simulation of rotational[17,30−32] and vibrational[29,31−33] spectra are of great help for the identification and analysis of either yet undetected or new/rare conformers. Moreover, for the "*in situ*" production of rare isomers,[34] for example via near-infrared (NIR) irradiation, the theoretical characterization of the best energy ranges able to excite specific overtone transitions and overcome the barriers

Received: June 19, 2015

DOI: 10.1021/acs.jctc.5b00580
J. Chem. Theory Comput. XXXX, XXX, XXX−XXX

between conformers facilitate the proper setup of such challenging experiments. In this context, the present investigation shows an effective computational strategy applied to a case study, namely, the structural and spectroscopic characterization of pyruvic acid.

The basic requirements for the theoretical support of new state-of-the-art experiments are the accurate predictions of (*i*) equilibrium molecular structures, (*ii*) free energies of different conformers for specific experimental conditions, and (*iii*) molecular spectra in the energy ranges of interest for all conformers and isotopologues possibly present in the experimental mixture. In all these cases, the target accuracy requires computations beyond the harmonic approximation, thus including vibrational anharmonic effects on rotational constants, thermodynamic properties, and on both line positions and intensities of IR spectra.

Concerning rotational spectra, the starting point is the computation of an accurate equilibrium geometry for the evaluation of the corresponding rotational constants.[35] Next, quadratic and cubic force constants allow the determination of vibrational corrections to rotational constants together with the quartic and sextic centrifugal-distortion constants.[36−39] Finally, accurate dipole moment components and, when needed, quadrupole-coupling constants complete the list of the needed quantities.[9,36] In our opinion, the most effective strategy relies on coupled-cluster (CC) evaluations (at the CC singles and doubles augmented by a perturbative treatment of triple excitations, CCSD(T)[40]) of equilibrium geometries, properties, and, possibly, quadratic force constants in a normal-mode representation (i.e., harmonic frequencies), also considering extrapolation to the complete basis set (CBS) limit and core−valence correlation (CV) contributions.[36,41−43] These results can be complemented by density functional theory (DFT) evaluations of the anharmonic contributions[33,44] (employing hybrid or double hybrid functionals, like B3LYP[45] and B2PLYP,[46] in conjunction with medium-sized basis sets). This strategy has been successfully applied, for example, to the investigation of the rotational spectra of thiouracil,[30] glycine dipeptide,[17] and the thiouracil−water complex.[47]

For larger molecules, benchmark studies suggest that the computationally expensive (and slowly converging) evaluation of harmonic frequencies at the CCSD(T)/CBS level augmented by CV corrections can be replaced by effective B2PLYP computations without any dramatic reduction of the accuracy[33,48,49] for both rotational and vibrational spectroscopy investigations. In this connection, it is noteworthy that more recent spin-component-scaled double hybrids, after heavy parametrization, provide with respect to B2PLYP improved thermochemical properties but essentially equivalent frequencies.[50] Furthermore, a very recent study[51] demonstrated that inclusion of post-MP2 contributions does not improve the results with respect to double hybrid functionals. Concerning vibrational spectroscopy, the simulation of fully anharmonic spectra including fundamental, overtones, and combination bands[33] requires, in addition to the quantities discussed above for the rotational spectra, quartic (at least semidiagonal) force constants together with second and third derivatives of the electric dipoles (for IR spectra). Once again, hybrid and double hybrid functionals perform very well in the computation of anharmonic contributions, provided that, for the evaluation of the electric dipoles, diffuse functions are properly included in the basis set.[33,49,52] Subsequently, the vibrational problem can be solved by either variational[53−68] or perturbative[69−100] approaches. For semirigid molecules, second-order vibrational perturbation theory (VPT2)[69,70] is particularly effective, provided that nearly resonant contributions are treated by means of a variational approach, thus leading to the so-called generalized VPT2 model (GVPT2),[75,80−82] also referred to as VPT2+WK.[96,97] In particular, a general VPT2 framework to compute thermodynamic properties, vibrational energies, and transition intensities for fundamentals, overtones, and combination bands,[80,81,91,93,94,99,100] also including reduced-dimensionality schemes for effective computations of large molecular systems,[101] simplifies the direct comparison with the experimental outcomes. In view of the identification of new species, such an approach permits distinguishing between low-intensity features related to nonfundamental transitions of the most abundant conformer and the fundamental transitions of the less abundant ones. This computational procedure can also be easily applied to a set of isotopologues with the aim of obtaining an unequivocal identification of several concomitantly present conformers when the situation is not so clear for the main isotopic species. Furthermore, the possibility of computing anharmonic spectra including combination bands up to three quanta paves the way to the detailed simulation of spectra over a large energy range, well within the near-infrared region. This general strategy has been successfully applied to the study of glycine,[33,102−105] acrolein,[106] and bibenzyl[107] conformers.

The approaches sketched above have led to the development of a virtual multifrequency spectrometer (VMS),[108,109] which consists of a comprehensive computational part providing access to the latest developments of computational spectroscopy (VMS-comp)[93,94,99,110−113] and a powerful graphical interface (VMS-draw),[114] the latter being able to pre- and postprocess the data, as well as to compare directly with the experimental spectra. The VMS-comp module in charge of vibrorotational spectroscopy beyond the harmonic level using VPT2[80,81,93,94,99] has been employed in the present study to evaluate the thermodynamic, kinetic, and spectroscopic properties of all pyruvic acid (PA) conformers (both those experimentally observed and those still elusive).

Regarding the molecule chosen in this study, PA is involved in several fundamental biological processes,[115] is widely used in industry,[116] and plays an important role in atmospheric reactions.[117,118] PA has two conformationally relevant internal degrees of freedom (see Figure 1), the rotations about the C−C bond between the carbonyl and carboxyl carbon atoms and about the C−O bond between the latter carbon atom and the oxidryl oxygen. According to theoretical predictions, this yields three different stable conformers in the ground electronic state.[29,119] These conformers, labeled as *Tc*, *Tt*, and *Ct*, following the nomenclature used in previous studies,[29,119,120] are depicted in Figure 1. The presence of those three conformers makes PA an ideal case study for demonstrating the suitability and reliability of our hybrid CC/DFT approach for the accurate determination of the molecular structures and spectroscopic properties of flexible molecules.

The microwave spectra of pyruvic acid have been already measured for several isotopic species of the most stable conformer *Tc*-PA[121] and for the lowest vibrational states of the main isotopologue.[122] However, the available data have not been applied to the determination of an accurate

DOI: 10.1021/acs.jctc.5b00580
J. Chem. Theory Comput. XXXX, XXX, XXX−XXX

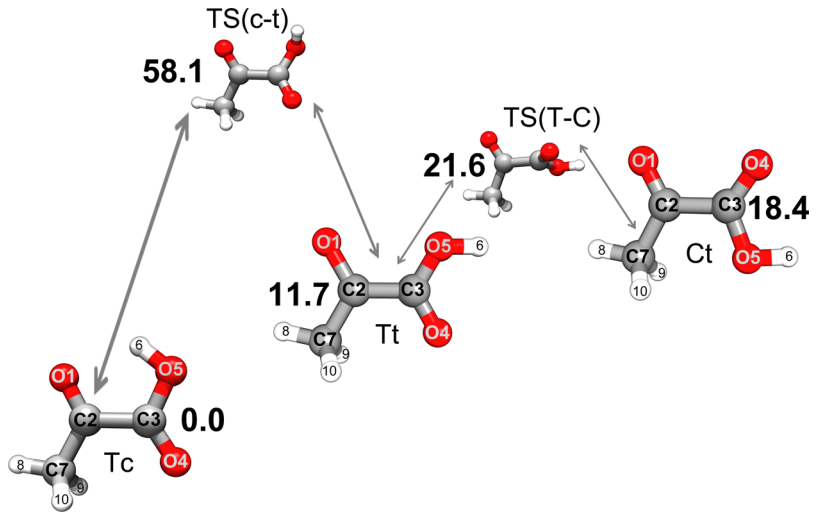

Figure 1. Molecular structure of the *Tc*-, *Tt*-, and *Ct*-pyruvic acid conformers and of the transition states for *Tc*-*Tt*, TS(c-t), and *Tt*-*Ct*, TS(C-T), isomerization. Atoms labeling and relative energies (in kJ mol^{-1}) computed at the CCSD(T)/CBS+CV level using the B2PLY/aug-cc-pVTZ equilibrium geometries are also reported. The upper-case letter (T, trans, = 180 deg and C, cis, = 0 deg) refers to the O1═C2−C3═O4 dihedral angle, and the lower-case letter (t, trans = 180 deg and c, cis = 0 deg) refers to the C2−C3−O5−H6 dihedral angle.

equilibrium structure within the so-called semiexperimental procedure[123] yet, and accurate estimates of the rotational constants for the two less stable conformers are still unknown. Concerning the vibrational spectrum of PA, the most recent characterization of different conformers[29] was performed in cryogenic argon and nitrogen matrices in the mid-IR and NIR regions. The investigation presented in ref 29 allowed the characterization of the spectroscopic features not only for the *Tc*-PA conformer but also for a second conformer (*Tt*-PA), which was produced in significant amounts by a selective NIR excitation of the first *Tc*-PA OH overtone that induced a large-scale conformational conversion. The subsequent selective NIR irradiation at the frequency of the first *Tt*-PA OH overtone led to a conversion back to *Tc*-PA, and no further conformers were observed. The IR characterization of *Tc*-PA and *Tt*-PA also comprises gas-phase measurements, in particular in the overtone range of the OH stretching vibrations.[124] The same two conformers were also observed in earlier IR experiments, where the *Tt*-PA conformer was either thermally populated in the gas phase[119] or generated by the UV-induced rotamerization.[125] On the other hand, the *Ct*-PA conformer, estimated to be less stable than *Tc*-PA by about 15−17 kJ mol^{-1},[29,119] has not been observed experimentally yet. On these grounds, the aim of the present study is to complete the characterization of all PA conformers and of the processes for their interconversion by means of the CC/DFT protocol introduced above.

The paper is organized as follows: first a detailed account of the methodology is presented in section 2, and then the results for equilibrium structures, energetic properties, and spectroscopic constants as well as rotational and IR spectra are presented and discussed in sections 3.1, 3.2, and 3.3.

2. METHODOLOGY

To characterize the stationary points on the potential energy surface (PES) and, in particular, to locate all energy minima and the first-order saddle points (transition states) connecting them, a preliminary investigation was carried at the DFT level. Within the DFT approach, the double-hybrid B2PLYP[44,46,126] functional was considered in conjunction with the aug-cc-pVTZ[127,128] basis set because of its accuracy and reliability in spectroscopic and structural studies.[44,49,106,129] Figure 1 depicts the minima located on the PES, namely, the *Tc*-, *Tt*-, and *Ct*-PA conformers, and the two transition states connecting them: TS(c-t) that connects the *Tc*- and *Tt*-PA conformers and TS(T-C) that connects *Tt*-PA and *Ct*-PA. Besides the characterization of the stationary points on the PES, DFT was used to compute harmonic and anharmonic force fields.[33] All DFT computations were performed employing the Gaussian suite of programs for quantum chemistry.[130]

In addition to the B2PLYP/aug-cc-pVTZ computations, the CCSD(T) method[40] and second-order Møller−Plesset perturbation theory (MP2)[131] were employed in molecular structure and property characterization as well as for harmonic force-field calculations, as described below. Correlation-consistent basis sets, (aug)-cc-p(C)V*n*Z (shortly denoted (A)(C)V*n*Z in Tables), with n = T, Q, 5,[127,128,132] were used in conjunction with the aforementioned methods. MP2 and CCSD(T) calculations were carried out with the quantum-chemical package Cfour.[133]

2.1. Molecular Structure and Energetics. For all conformers, an accurate structural determination of the three minima located on the PES was carried out by accounting simultaneously for basis-set effects as well as core-correlation contributions at an energy-gradient level. We made use of the composite scheme presented in refs 41 and 42 and implemented in Cfour. The overall gradient employed in the geometry optimization was therefore given by

$$\frac{dE_{CBS+CV}}{dx} = \frac{dE^{CBS}(HF-SCF)}{dx} + \frac{d\Delta E^{CBS}(CCSD(T))}{dx} + \frac{d\Delta E(CV)}{dx} \quad (1)$$

where CBS denotes the complete basis set limit, and CV denotes the core−valence correlation correction; $dE^{CBS}(HF\text{-}SCF)/dx$ and $d\Delta E^{CBS}(CCSD(T))/dx$ are the energy gradients corresponding to the exp(−*Cn*) extrapolation scheme for HF-

DOI: 10.1021/acs.jctc.5b00580
J. Chem. Theory Comput. XXXX, XXX, XXX−XXX

SCF[134] and to the n^{-3} extrapolation formula for the CCSD(T) correlation contribution,[135] respectively. In the expression given above, n = T, Q, and 5 were chosen for the HF-SCF extrapolation, and n = T and Q were used for CCSD(T). The core-correlation energy correction, ΔE(CV), was obtained as the difference of all-electron and frozen-core CCSD(T) calculations using the core−valence cc-pCVTZ basis set.[132] This approach exclusively relies on CCSD(T) calculations and, in the following, will be denoted as "best CC".

The results of the composite approach described above provide the opportunity to further test a computational scheme that has been recently introduced to obtain accurate equilibrium structures of medium-sized molecules[30,105] and has been denoted as "cheap"[49] to stress the reduced computational cost. This approach is based on corrections on top of the CCSD(T)/cc-pVTZ level, which are applied directly to the geometrical parameters. The contributions considered are the basis-set extrapolation to the CBS limit, Δr(CBS), and the core-correlation effects, Δr(CV), both computed at the MP2 level.[131] The structural parameters were determined as

$$r(\text{best}) = r(\text{CCSD(T)/VTZ}) + \Delta r(\text{CBS}) + \Delta r(\text{aug}) + \Delta r(\text{CV}) \quad (2)$$

where Δr(aug) denotes the correction due to the inclusion of diffuse functions in the basis set and is an empirical trick to recover the overestimation of the extrapolation to the CBS limit due to the use of rather small sets (n = T and Q) and to the application of the n^{-3} extrapolation formula[135] to the entire geometrical parameters (and not only to the correlation contribution; see ref 136 for all details). Despite being empirical in nature, this approach is nowadays rather well tested.[17,47,49,105,136−138] In the following, the results obtained by means of this composite scheme will be denoted as "best cheap".

For the determination of the conformational enthalpy, a composite scheme analogous to that of eq 1 was employed to evaluate best estimates of the total electronic energies, shortly denoted as CCSD(T)/CBS+CV in the text and tables. Calculations were performed at the "best CC", "best cheap", and B2PLYP/aug-cc-pVTZ optimized geometries. To accurately determine the energy barrier for the *Tc-Tt* and *Tt-Ct* interconversions, CCSD(T)/CBS+CV energy computations were also carried out at the B2PLYP/aug-cc-pVTZ transition-state structures. The CCSD(T)/CBS+CV relative energies also provide the opportunity to test the accuracy of the energetic properties computed at the B2PLYP/aug-cc-pVTZ level. The required thermodynamic properties were computed beyond the harmonic approximation by means of simple perturbation theory (SPT)[93,139] combined with the Hindered-Rotor Anharmonic Oscillator (HRAO) model,[93,140] as explained later in the 2.3 section.

2.2. Harmonic and Anharmonic Force Fields. As briefly mentioned above, for all conformers, the best-estimated harmonic force fields were evaluated by means of the so-called "best cheap" composite scheme. This implied the evaluation of harmonic force fields at the same level of theory as the corresponding optimized geometries (i.e., at the CCSD(T)/cc-pVTZ, MP2/cc-pVTZ, MP2/cc-pCVTZ —all electrons and frozen-core— and MP2/aug-cc-pVTZ levels) using analytic second derivatives.[141] For an exhaustive account on this approach, the reader is referred, for example, to ref 105.

Anharmonic force-field computations were carried out at the B2PLYP/aug-cc-pVTZ level. The cubic and semidiagonal quartic force fields and up to the third derivatives of the electric dipole moment were determined by numerical differentiations of analytic force constants[44] and first derivatives of the electric dipole at displaced geometries along the normal modes (with a 0.01 Å step), with the equilibrium structure optimized using tight convergence criteria (maximum forces and displacements smaller than 1.5×10^{-5} Hartree/Bohr and 6×10^{-5} Å, respectively).

To further improve the description of the anharmonic force field, a hybrid model was used, which assumes that the differences between vibrational frequencies computed at two different levels of theory are mainly due to the harmonic terms. This approach is already well-tested for small closed- and open-shell molecular systems (see, for instance, refs 49, 93, and 142−145). For all conformers, the hybrid force fields were obtained in a normal-coordinate representation by adding the cubic and semidiagonal quartic B2PLYP/aug-cc-pVTZ force constants to the "best cheap" harmonic frequencies. When the normal modes are very similar, as in the present case, DFT cubic and quartic force constants can be used without any transformation.

2.3. VPT2 Computations of Vibrational Energies and IR Intensities. The computations of vibrational spectra beyond the double-harmonic approximation, of the vibrational corrections to rotational constants and molecular properties (*vide infra*), as well as of the Zero Point Vibrational (ZPV) contributions to the conformational energy were obtained within the VPT2 approach.[69,70] In particular, thermodynamic properties, vibrational frequencies, and intensities for fundamentals, overtones, and combination bands were derived by using a general VPT2 platform[80,81,91,93,94,99,100] developed and implemented in the GAUSSIAN suite of programs for quantum chemistry[130] by some of the present authors. VPT2 calculations were carried out using both the B2PLYP/aug-cc-pVTZ and hybrid "best cheap"/B2PLYP anharmonic force fields.

To overcome the problem of singularities (known as resonances) plaguing the VPT2 approach, the Fermi resonances have been treated within the GVPT2 scheme, where the nearly resonant contributions are removed from the perturbative treatment (leading to the deperturbed model, DVPT2) and variationally treated in a second step.[75,80,82,100] Such an approach relies on semiempirical thresholds for first-order resonances. In the present work, the procedure proposed by Martin et al.[82] for the identification of Fermi resonances were chosen, associated with the preliminary check on the frequency difference at the denominator.[80] Recently, our tool has been extended to compute anharmonic intensities (IR, vibrational circular dichroism (VCD) and Raman) for the fundamentals, overtones, and combination bands up to three quanta.[33,91,94,99,102] The computation of IR intensities employs the default thresholds for 1−1 and 1−3 resonances, as proposed by some of us,[94,99] that are known to lead to very good results for wavenumbers and IR intensities of fundamental transitions,[33,49,146] overtones, and combination bands.[29,52,99,147] In analogy to frequencies, a successive variational correction is applied to the DVPT2 transition moments, by projecting them on the vibrational wave

DOI: 10.1021/acs.jctc.5b00580
J. Chem. Theory Comput. XXXX, XXX, XXX−XXX

functions obtained from the variational treatment of the energy.[90]

For all conformers, the hybrid force fields were also employed to compute resonance-free hybrid degeneracy-corrected VPT2 (HDCPT2)[93] vibrational wavenumbers and ZPV[148] energies, which were subsequently used in the evaluation of thermodynamic properties. For the proper treatment of torsional anharmonicity, which represents a challenging aspect for accurate thermochemical calculations of complex molecules,[140,149,150] we employed a Hindered-Rotor Anharmonic Oscillator (HRAO) model, which is a generalization of the Hindered-Rotor Harmonic Oscillator approach.[140] The HRAO model automatically identifies internal rotation modes and rotating groups in the normal-mode vibrational analysis and employs an effective analytical approximation of the partition function for a one-dimensional hindered internal rotation. The contributions of the remaining modes are then computed by means of HDCPT2 coupled to the SPT approach to the partition function.[93] In the specific case of the pyruvic acid, for all conformers, the two lowest energy vibrations were treated as hindered rotations.

All VPT2 computations were performed employing the development version of GAUSSIAN suite of programs for quantum chemistry.[130] VMS-Draw[114] was used to visualize the normal modes, analyze in detail the outcome of vibrational computations, and plot IR spectra.

2.4. Rotational Spectroscopy Parameters. The equilibrium rotational constants were straightforwardly derived from the corresponding equilibrium structure[36,151] at the "best CC" level and subsequently corrected for vibrational effects. The corresponding corrections, $\Delta B^i_{\mathrm{vib}}$, were obtained within VPT2 from the following expression[69,70]

$$\Delta B^i_{\mathrm{vib}} = -\frac{1}{2}\sum_s \alpha^i_s \tag{3}$$

where $\alpha^{i\prime}_s$s are the vibration−rotation interaction constants, with s and i denoting the normal mode and the inertial axis, respectively. The required semidiagonal cubic force field was computed at the "best cheap"/B2PLYP level of theory.

By making use of the harmonic force fields evaluated at different levels of theory (i.e., in the frame of the so-called "best cheap" scheme), best estimates for quartic centrifugal-distortion constants, D(best), were derived as follows

$$\begin{aligned} D(\mathrm{best}) = {} & D(\mathrm{CCSD(T)/VTZ}) \\ & + [D(\mathrm{MP2/CVTZ, all}) - D(\mathrm{MP2/CVTZ, fc})] \\ & + [D(\mathrm{MP2/augVTZ, fc}) - D(\mathrm{MP2/VTZ, fc})] \\ & + [D(\mathrm{MP2/VQZ, fc}) - D(\mathrm{MP2/VTZ, fc})] \end{aligned} \tag{4}$$

where D denotes a generic quartic centrifugal-distortion constant. The first difference (in square brackets) provides the CV correction (ΔD(CV)), the second one the contribution of diffuse functions (ΔD(aug)), and the last one the effect of enlarging the basis set from triple- to quadruple-ζ. Watson's A-reduced Hamiltonian in the I^r representation[152] has been employed. Within such a reduction, sextic centrifugal-distortion constants were also computed using the "best cheap"/B2PLYP and B2PLYP/aug-cc-pVTZ cubic force fields.

For all conformers, the components of the equilibrium electric dipole moment (required to predict the intensity of rotational transitions) were computed by means of a composite scheme analogous to that employed for the "cheap" molecular structure determination. The approach is described in detail, for example, in ref 104, and involves an extrapolation to the CBS limit and the inclusion of core-correlation and diffuse-function corrections. The vibrational ground-state dipole moment components were then obtained by combining the best-estimated equilibrium values with vibrational contributions evaluated at the "best cheap"/B2PLYP level. The latter corrections were determined by performing a vibrational averaging of the molecular property by means of VPT2, as implemented in GAUSSIAN.[80,81,94,130]

2.4.1. Semiexperimental Approach. Taking advantage of the availability of the experimental ground-state rotational constants for all singly and one multiply substituted isotopic species of the most stable (*Tc*-PA) conformer of pyruvic acid,[121,122] the so-called semiexperimental equilibrium structure,[123] r_e^{SE}, was obtained in the present study. The procedure involves a least-squares fit of the structural parameters to the equilibrium moments of inertia, I^i_e, the latter being straightforwardly derived from the corresponding semiexperimental equilibrium rotational constants, B^i_e. These are obtained by correcting the experimental ground-state constants, B^i_0, for the vibrational and electronic effects

$$B^i_e = B^i_0 - \Delta B^i_{\mathrm{vib}} - \Delta B^i_{\mathrm{el}} \tag{5}$$

where $\Delta B^i_{\mathrm{vib}}$ is the vibrational correction introduced in eq 3, and ΔB^i_{el} is the electronic correction. The latter is connected to the rotational g-factor (see, for example, refs 36,151, and 153)

$$\Delta B^\beta_{\mathrm{el}} = -\frac{m_{\mathrm{e}}}{M_{\mathrm{p}}} g_{\beta\beta} B^\beta_e \tag{6}$$

where m_{e} and M_{p} are the masses of the electron and proton, respectively. The rotational g-tensor and the corresponding electronic corrections to rotational constants for the various isotopic species were computed at the B3LYP/aug-cc-pVTZ level. The least-squares fit was performed using the I^A_e and I^C_e moments of inertia, and the weighting scheme was chosen in order to have the moments of inertia equally weighted. The isotopic species considered were $CH_3COCOOH$, $CH_3C^{18}OCOOH$, $CH_3COC^{18}OOH$, $CH_3COCO^{18}OH$, $^{13}CH_3COCOOH$, $CH_3{}^{13}COCOOH$, $CH_3CO^{13}COOH$, $CD_3COCOOH$, $CDH_2COCOOH$, and $CH_3COCOOD$. In addition, since the experimental rotational constants of $CH_3COC^{18}OOH$, $CH_3COCO^{18}OH$, and $CH_3COCOOD$ are affected by large uncertainties, only their I^B_e inertia moments were included in the fit, thus allowing to consider their contribution.

The well documented accuracy of the semiexperimental equilibrium structure (see, for instance, refs 36, 154, and 155) is leading to its systematic use as reference in benchmark studies (see, for example, refs 35, 49, 105, and 156−158). In the present work it was furthermore used to correct the geometries of the *Tt*- and *Ct*-PA conformers. In the frame of the so-called "template-molecule" (TM) approach,[155] the r_e^{SE} structure is used as a template for deriving the corrections to geometrical parameters for similar molecules (e.g., conformers or substituted systems)

$$r_e(\mathrm{corrected}) = r_e + \Delta\mathrm{TM} \tag{7}$$

where ΔTM is defined as

DOI: 10.1021/acs.jctc.5b00580
J. Chem. Theory Comput. XXXX, XXX, XXX−XXX

Table 1. Equilibrium Structure (Distances in Å, Angles in deg) and Rotational Constants (in MHz) of *Tc*-Pyruvic Acid

parameters	B2PLYP/VTZ	B2PLYP/AVTZ	CCSD(T) VTZ	"best cheap"[a]	"best CC"[b]	semiexp[c] r_e^{SE}	exp[d] r_s
Bonds							
C2═O1	1.2153	1.2154	1.2179	1.2109	1.2114	1.2115(5)	1.231(5)
C2−C3	1.5434	1.5450	1.5430	1.5409	1.5387	1.5382(8)	1.523(3)
C2−C7	1.4916	1.4911	1.4972	1.4894	1.4893	1.4899(7)	1.486(4)
C3═O4	1.2021	1.2027	1.2036	1.1983	1.1979	1.1979(5)	1.215(5)
C3−O5	1.3346	1.3350	1.3370	1.3296	1.3297	1.3312(6)	1.328(5)
O5−H6	0.9746	0.9748	0.9739	0.9709	0.9706	0.9678(4)	0.983(5)
C7−H8	1.0845	1.0846	1.0871	1.0847	1.0845	1.0819(5)	1.074(2)
C7−H9(H10)	1.0896	1.0898	1.0916	1.0896	1.0893	1.0902(2)	1.106(6)
MAE wrt SE[e]	0.0035	0.0038	0.0053	0.0015	0.0011		0.012
|MAX|wrt SE[e]	0.0068	0.0070	0.0074	0.0031	0.0029		0.020
MAE wrt "best CC"[f]	0.0030	0.0034	0.0050	0.0005			0.012
|MAX|wrt "best CC"[f]	0.0049	0.0063	0.0079	0.0023			0.020
Angles							
C3−C2═O1	117.80	117.74	117.83	117.69	117.70	117.75(5)	117.0(1.6)
C7−C2═O1	125.22	125.29	125.36	125.47	125.39	125.32(5)	124.4
O4═C3−C2	123.10	123.07	122.91	122.71	122.80	122.88(5)	122.0(1.8)
O5−C3═O4	124.45	124.22	124.57	124.10	124.38	124.32(5)	123.5
H6−O5−C3	106.03	106.57	105.29	107.22	106.40	106.40(2)	105.2(1.9)
H8−C7−C2	110.06	110.05	109.88	109.82	109.88	110.19(4)	110.7(1.1)
H9(H10)−C7−C2	109.51	109.48	109.34	109.28	109.35	109.26(2)	109.0(2.6)
H9−C7−C2═O1	121.99	121.99	121.86	121.89	121.92	122.20(4)	
H10−C7−C2═O1	−121.99	−121.99	−121.86	−121.89	−121.92	−122.20(4)	
MAE wrt SE[e]	0.17	0.13	0.26	0.24	0.12		0.67
|MAX| wrt SE[e]	0.37	0.22	1.11	0.83	0.31		1.20
MAE wrt "best CC"[f]	0.15	0.12	0.17	0.15			0.72
|MAX| wrt "best CC"[f]	0.37	0.27	1.11	0.82			1.20
Rotational Constants							
A_e/MHz	5528.271	5530.082	5501.828	5564.497	5560.694	5559.272	
B_e/MHz	3602.986	3593.742	3602.386	3611.364	3623.700	3621.518	
C_e/MHz	2210.511	2207.344	2206.303	2219.597	2223.580	2222.430	

[a]Best estimate from eq 2. [b]Best estimate from eq 1. [c]B_0 from ref 121 and vibrational corrections at the B2PLYP/aug-cc-pVTZ level. Given uncertainties are three times the standard deviation of the fit. [d]Substitution structure: ref 121. [e]Mean absolute error (MAE) and maximum absolute deviations (|MAX|) with respect to the semiexperimental equilibrium structure. [f]Mean absolute error (MAE) and maximum absolute deviations (|MAX|) with respect to the best-estimated ("best CC") parameters.

$$\Delta TM = r_e^{SE}(TM) - r_e(TM) \quad (8)$$

and r_e is the geometrical parameter of interest calculated at the same level of theory for both the molecule under consideration and the one chosen as reference, the so-called template molecule. The pyruvic acid provides the opportunity to further check the reliability of the TM approach by applying ΔTM corrections to the "best CC", "best cheap", and B2PLYP/aug-cc-pVTZ equilibrium structures of the *Tt*-PA and *Ct*-PA conformers.

3. RESULTS AND DISCUSSION

3.1. Characterization of the Stationary Points. The results for the molecular structure determination of *Tc*-, *Tt*-, and *Ct*-PA are summarized in Tables 1, 2, and 3, respectively, with the atoms labeled according to Figure 1.

First of all, we point out that the semiexperimental equilibrium structure was determined for *Tc*-PA with a root-mean-square (RMS) of the residuals (in terms of equilibrium rotational constants) of 0.0008 MHz, which is, together with the small uncertainties shown in Table 1, an indicator of the good quality of the fitted geometry. The reliability of the derived r_e^{SE} structure allows us to estimate the accuracy of theoretical equilibrium structures computed at different levels of theory. For instance, we note that the "best CC" eq 1 and semiexperimental parameters show mean differences of 0.0011 Å and 0.12 deg for bond lengths and angles, respectively. This good agreement therefore confirms the typical accuracy of the so-called "best CC" structures, also denoted as CCSD(T)/CBS+CV, that can be inferred from the literature on this topic (see, for example, refs 36, 41, 42, 105, and 159). Similarly, it is worthwhile noting the good performance of the so-called "best cheap" composite scheme, which provides structural parameters with mean absolute errors (MAE, with respect to the semiexperimental equilibrium structure) of 0.0015 Å for bond lengths and 0.24 deg for bond angles. Moreover, for all conformers, the "best cheap" approach provides results in very good agreement with the "best CC" one in spite of its considerably lower computational cost, as indicated by MAEs smaller than 0.001 Å and 0.15 deg for bond lengths and angles, respectively.

B2PLYP/aug-cc-pVTZ also performs very well and at a significantly lower computational cost. In particular, both the B2PLYP/aug-cc-pVTZ and B2PLYP/cc-pVTZ levels of theory yield significantly better results than CCSD(T)/cc-pVTZ for the equilibrium structure determination of *Tc*-PA. Furthermore, for all conformers the B2PLYP/aug-cc-pVTZ level of theory provides structural parameters with a MAE with

DOI: 10.1021/acs.jctc.5b00580
J. Chem. Theory Comput. XXXX, XXX, XXX−XXX

Table 2. Equilibrium Structure (Distances in Å, angles in deg) and Rotational Constants (in MHz) of *Tt*-Pyruvic Acid

	B2PLYP/AVTZ		"best cheap"[a]		"best CC"[b]	
parameters	r_e	r_e+ΔTM[c]	r_e	r_e+ΔTM[c]	r_e	r_e+ΔTM[c]
Bonds						
C2═O1	1.2071	1.2033	1.2040	1.2046	1.2039	1.2041
C2−C3	1.5440	1.5373	1.5392	1.5365	1.5370	1.5366
C2−C7	1.4993	1.4982	1.4966	1.4972	1.4969	1.4976
C3═O4	1.2078	1.2031	1.2035	1.2032	1.2032	1.2032
C3−O5	1.3383	1.3346	1.3321	1.3338	1.3324	1.3340
O5−H6	0.9689	0.9619	0.9656	0.9625	0.9651	0.9623
C7−H8	1.0847	1.0820	1.0847	1.0820	1.0846	1.0821
C7−H9(H10)	1.0896	1.0900	1.0895	1.0901	1.0891	1.0901
MAE wrt best CC[d]	0.0034		0.0005			
|MAX|wrt best CC[d]	0.0070		0.0022			
MAE wrtbest CC+ΔTM[e]		0.0004		0.0002		
|MAX|wrt best CC+ΔTM[e]		0.0008		0.0006		
Angles						
C3−C2═O1	120.38	120.39	120.18	120.25	120.29	120.35
C7−C2═O1	124.92	124.95	124.98	124.84	124.97	124.90
O4═C3−C2	122.85	122.66	122.45	122.62	122.58	122.66
O5−C3═O4	124.69	124.80	124.89	125.12	124.76	124.70
H6−O5−C3	106.95	106.78	107.12	106.30	106.59	106.60
H8−C7−C2	109.38	109.52	109.19	109.56	109.23	109.54
H9(H10)−C7−C2	109.91	109.69	109.71	109.69	109.80	109.71
H9−C7−C2═O1	121.61	121.83	121.54	121.85	121.56	121.84
H10−C7−C2═O1	−121.61	−121.83	−121.54	−121.85	−121.56	−121.84
MAE wrt best CC[d]	0.13		0.12			
|MAX|wrt best CC[d]	0.36		0.52			
MAE wrt best CC+ΔTM[e]		0.05		0.11		
|MAX|wrt best CC+ΔTM[e]		0.19		0.41		
Rotational Constants						
A_e/MHz	5631.076		5664.408		5666.384	
B_e/MHz	3484.687		3508.343		3512.296	
C_e/MHz	2181.103		2195.481		2197.263	

[a]Best estimate from eq 2. [b]Best estimate from eq 1. [c]Theoretical equilibrium structure corrected according to eq 8. [d]Mean absolute error (MAE) and maximum absolute deviations (|MAX|) with respect to the ("best CC") parameters. [e]Mean absolute error (MAE) and maximum absolute deviations (|MAX|) with respect to the best-estimated ("best CC"+ΔTM) parameters.

respect to the "best CC" values always within 0.0035 Å and 0.13 deg for bond lengths and angles, respectively. While the accuracy of bond angles can be considered on average fully satisfactory, some systematic deviations are observed for the distances, i.e., all bond lengths except C−H are overestimated by 0.002−0.006 Å. These results can be improved by means of the TM approach, i.e., by correcting the geometrical parameters of *Tt*-PA and *Ct*-PA conformers for the differences between theoretical and semiexperimental parameters observed for their *Tc*-PA counterparts. From Tables 2 and 3 it is evident that the TM approach essentially provides the same equilibrium structure (i.e., bond distances well within 0.001 Å) independently of the level of theory considered, namely, "best CC", "best cheap", and B2PLYP/aug-cc-pVTZ, and irrespectively of the larger intrinsic errors of the DFT one. For these reasons, the B2PLYP/aug-cc-pVTZ level of theory represents a good compromise between computational cost and accuracy, thus allowing reliable calculations for significantly larger systems that can be further improved using the TM scheme. This finding supports our choice of computing the transition state structures only at the B2PLYP/aug-cc-pVTZ level.

Finally, we comment on the comparison of our semiexperimental equilibrium structure r_e^{SE} with the pure experimental molecular geometry available. In Table 1, the substitution structure (r_s)[121] obtained by means of Costain's method[160] directly applied to the vibrational ground-state rotational constants is also reported. As well-known (see, for instance, refs 36 and 38), this approach presents severe limitations in properly describing the equilibrium geometry. In the present case, this is confirmed by the large discrepancies noted between the r_e^{SE} and r_s parameters as well as by the large uncertainties affecting the latter, which are one order of magnitude larger than those affecting the r_e^{SE} parameters.

The relative energies of the minima structures are collected in Table 4 together with the interconversion barriers (ruled by the TS(*c*-*t*) and TS(*T*-*C*) transition states, see Figure 1). For all minima, the relative energies were computed at the CCSD(T)/CBS+CV and B2PLYP/aug-cc-pVTZ levels using the B2PLYP/aug-cc-pVTZ, "best cheap", and "best CC" optimized structures. For the transition states, only the B2PLYP/aug-cc-pVTZ optimized geometries were considered, which are listed in Table 5. For all reference structures used in the calculation, the CCSD(T)/CBS+CV relative energies of *Tc*-PA, *Tt*-PA, and *Ct*-PA agree within 0.06 kJ mol^{-1}. In particular, the B2PLYP/aug-cc-pVTZ level provides good reference structures for accurate thermochemical computations, showing in the present case an agreement within 0.01

DOI: 10.1021/acs.jctc.5b00580
J. Chem. Theory Comput. XXXX, XXX, XXX−XXX

Table 3. Equilibrium Structure (Distances in Å, Angles in deg) and Rotational Constants (in MHz) of *Ct*-Pyruvic Acid

	B2PLYP/AVTZ		"best cheap"[a]		"best CC"[b]	
parameters	r_e	r_e+ΔTM[c]	r_e	r_e+ΔTM[c]	r_e	r_e+ΔTM[c]
Bonds						
C2═O1	1.2056	1.20174	1.2024	1.2030	1.2025	1.2027
C2−C3	1.5511	1.54438	1.5462	1.5435	1.5437	1.5433
C2−C7	1.5014	1.50023	1.4989	1.4995	1.4990	1.4997
C3═O4	1.1992	1.19448	1.1946	1.1942	1.1948	1.1948
C3−O5	1.3538	1.35007	1.3479	1.3496	1.3475	1.3491
O5−H6	0.9692	0.96216	0.9660	0.9629	0.9653	0.9625
C7−H8	1.0851	1.08237	1.0850	1.0823	1.0849	1.0823
C7−H9(H10)	1.0897	1.09008	1.0895	1.0901	1.0892	1.0902
MAE wrt best CC[d]	0.0035		0.0006			
|MAX|wrt best CC[d]	0.0074		0.0025			
MAE wrt best CC+ΔTM[e]		0.0006		0.0003		
|MAX|wrt best CC+ΔTM[e]		0.0011		0.0006		
Angles						
C3−C2═O1	117.78	117.79	117.75	117.8235	117.81	117.86
C7−C2═O1	124.33	124.37	124.40	124.2591	124.37	124.30
O4═C3−C2	124.28	124.09	124.31	124.4864	124.24	124.32
O5−C3═O4	124.23	124.33	124.41	124.6397	124.30	124.24
H6−O5−C3	107.02	106.84	107.08	106.2630	106.68	106.69
H8−C7−C2	109.26	109.40	109.08	109.4531	109.08	109.39
H9(H10)−C7−C2	110.08	109.86	109.90	109.8804	109.98	109.90
H9−C7−C2═O1	121.38	121.60	121.31	121.6234	121.33	121.61
H10−C7−C2═O1	−121.38	−121.60	−121.31	−121.6234	−121.33	−121.61
MAE wrt best CC[d]	0.10		0.09			
|MAX|wrt best CC[d]	0.33		0.40			
MAE wrt best CC+ΔTM[e]		0.05		0.13		
|MAX|wrt best CC+ΔTM[e]		0.14		0.42		
Rotational Constants						
A_e/MHz	5560.910		5590.132		5593.588	
B_e/MHz	3487.960		3514.914		3518.337	
C_e/MHz	2171.850		2186.854		2188.650	

[a]Best estimate from eq 2. [b]Best estimate from eq 1. [c]Theoretical equilibrium structure corrected according to eq 8. [d]Mean absolute error (MAE) and maximum absolute deviations (|MAX|) with respect to the ("best CC") parameters. [e]Mean absolute error (MAE) and maximum absolute deviations (|MAX|) with respect to the best-estimated ("best CC"+ΔTM) parameters.

Table 4. Electronic Energies of the *Tc*-, *Tt*-, and *Ct*-PA Conformers and Corresponding Transition States

computational model			ΔE wrt *Tc*-PA [kJ mol^{-1}]			
geometry	energy	energy [au] *Tc*-PA	*Tt*-PA	*Ct*-PA	TS(c-t)	TS(T-C)
B2PLYP/AVTZ	B2PLYP/AVTZ	−342.307881	11.41	18.10	58.34	20.11
B2PLYP/AVTZ	B2PLYP-D3/AVTZ	−342.313243	11.69	18.35	58.55	20.39
B2PLYP-D3/AVTZ	B2PLYP-D3/AVTZ	−342.313244	11.69	18.34	58.97	20.44
B2PLYP/AVTZ	CCSD(T)/CBS+CV	−342.388266	11.68	18.45	58.07	21.57
"best cheap"[a]	CCSD(T)/CBS+CV	−342.388379	11.62	18.39		
"best CC"[b]	CCSD(T)/CBS+CV	−342.388411	11.67	18.45		

[a]Best estimate from eq 2. [b]Best estimate from eq 1.

kJ mol^{-1} with the best theoretical estimates, further validating its application in transition state computations. Furthermore, we note the good accuracy of the relative energies computed at the B2PLYP/aug-cc-pVTZ level with respect to CCSD(T)/CBS+CV, with an agreement within 0.35 kJ mol^{-1} for minima and 1.5 kJ mol^{-1} for transition states. In all cases, the agreement is improved by adding a semiempirical dispersion correction (D3)[161] that reduces the discrepancies to 0.1 kJ mol^{-1} and 1.2 kJ mol^{-1} for minima and transition states, respectively. We note that for PA, the dispersion correction does not introduce significant structural changes neither for the minima nor for the transition states, with the only noticeable differences (1−2 deg) observed for the O5−C3−C2−O1 dihedral angle of the transition states. However, the B2PLYP-D3 scheme is recommended, in particular for larger and more complex systems, as demonstrated for medium-sized molecules including hydrogen bonding and flexible side chains.[162,163]

In Table 6, the best estimates of the gas-phase thermodynamic properties of the PA conformers at 15, 298.15, 328, and 480 K are also given. These temperatures were selected because they were employed in IR[29,119,124] and microwave[121,122] experiments of relevance to the present work. It is noteworthy that the widely used rigid-rotor

DOI: 10.1021/acs.jctc.5b00580
J. Chem. Theory Comput. XXXX, XXX, XXX−XXX

Table 5. Equilibrium Structures (Distances in Å, Angles in deg) of the TS(c-t) and TS(T-C) Transition States Computed at the B2PLYP/aug-cc-pVTZ Level

parameters	TS(c-t)	TS(T-C)
Bonds		
C2═O1	1.2097	1.2083
C2−C3	1.5428	1.5343
C2−C7	1.4982	1.5006
C3═O4	1.1996	1.2024
C3−O5	1.3634	1.3490
O5−H6	0.9636	0.9703
C7−H8	1.0849	1.0855
C7−H9	1.0906	1.0902
C7−H10	1.0891	1.0910
Angles		
C3−C2═O1	118.80	118.82
C7−C2═O1	125.01	124.99
O4═C3−C2	121.68	124.16
O5−C3═O4	124.06	124.72
H6−O5−C3	112.30	107.42
H8−C7−C2	109.73	109.83
H9−C7−C2	109.73	109.57
H10−C7−C2	109.64	109.57
O5−C3−C2−O1	−32.29	−109.46
H6−O5−C3−C2	93.53	178.40
H9−C7−C2═O1	123.86	120.19
H10−C7−C2═O1	−119.34	−122.36

Table 6. Theoretical Thermodynamic Properties[a] (kJ mol^{-1}) of the Pyruvic Acid Conformers

temperature	parameter	*Tc*-PA	*Tt*-PA	*Ct*-PA
	ΔE_{ele}[b]/kJ mol^{-1}	0.00	11.67	18.45
	ΔE_{ZPVE}[c]/kJ mol^{-1}	0.00	10.83	17.41
T = 15 K	ΔH[d]/kJ mol^{-1}	0.00	10.84	17.44
	ΔG[d]/kJ mol^{-1}	0.00	10.83	17.39
	Pop (%)	100.0	0.0	0.0
T = 298.15 K	ΔH[d]/kJ mol^{-1}	0.00	11.50	17.32
	ΔG[d]/kJ mol^{-1}	0.00	8.82	14.90
	Pop (%)	97.0	2.8	0.2
T = 328 K	ΔH[d]/kJ mol^{-1}	0.00	11.53	17.29
	ΔG[d]/kJ mol^{-1}	0.00	8.55	14.66
	Pop (%)	95.4	4.1	0.4
T = 480 K	ΔH[d]/kJ mol^{-1}	0.00	11.45	16.98
	ΔG[d]/kJ mol^{-1}	0.00	7.18	13.49
	Pop (%)	83.4	13.8	2.8

[a]All thermodynamic properties were computed at 1 atm. [b]Best-estimated CCSD(T)/CBS + CV electronic energies computed at the "best CC" equilibrium geometries eq 1. [c]Anharmonic resonance-free[100,148] ZPV energies computed using the hybrid "best cheap"/B2PLYP force field for the *Tc*-PA (185.63 kJ mol^{-1}), *Tt*-PA (184.79 kJ mol^{-1}) and *Ct*-PA (184.59 kJ mol^{-1}). [d]Contributions computed by means of the HRAO model using the hybrid "best cheap"/B2PLYP force field, in conjunction with HDCPT2 computations and simple perturbation theory (SPT). The two lowest vibrations were described by hindered-rotor contributions computed by an automatic procedure. See text for all details.

harmonic oscillator model (RRHO) yields thermodynamic properties in qualitative agreement with the full HRAO approach also at the highest temperatures under consideration here, with the differences in relative free energies and Boltzmann populations being within 1 kJ mol^{-1} and 1%, respectively. However, RRHO might provide unrealistic free energies, as it was the case of the IIIp/tct glycine conformer at 410 K because of the overestimation of entropic effects.[105] These results were corrected by applying the more realistic HRAO model, which was therefore preferred in the present study.

The results of Table 6 confirm the stability order pointed out in some previous works;[29,119,125] however, both *Tt*-PA and *Ct*-PA conformers are predicted to be slightly less stable (by about 2 kJ mol^{-1}) than what previously reported, the best-estimated relative energies with respect to the *Tc*-PA conformer being 11.67 and 18.45 kJ mol^{-1}, respectively. These results lead to conformational enthalpies of 11.5 and 17.3 kJ mol^{-1} at room temperature and of 10.8 and 17.3 kJ mol^{-1} at 15 K for *Tt*-PA and *Ct*-PA, respectively. For *Tt*-PA, these values agree reasonably well with the experimental estimates of 8.7(±1.3) kJ mol^{-1} and 9.4(±1.4) kJ mol^{-1} from low-temperature matrix[119] and gas-phase studies,[164] respectively. The present theoretical results and, in particular, the relative stabilities of the minima and the barrier height for TS(*c-t*) are fully in line with the recent discussion of the reversible interconversion processes of *Tc*-PA to *Tt*-PA reported in ref 29. Our results also show that TS(*c-t*) is obtained by rotation of the OH group, as indicated by the corresponding transition vector (with imaginary frequency of *i*630 cm^{-1}) with structural changes due to the O5−C3−C2−O1 and H6−O5−C3−C2 dihedral angles.

Concerning the possible detection of the elusive *Ct*-PA conformer, our results indicate that it should be thermally populated up to about 3% at 480 K, but its detection is complicated by the low-energy barrier for the conversion toward *Tt*-PA and by the conformational cooling effect, which in fact prevented the survival of *Ct*-PA during its deposition in a cryogenic matrix at 15 K.[29] On the other hand, the detection of *Ct*-PA could be feasible in gas-phase experiments based on jet-cooled molecular beams, in particular close to the entrance of the nozzle, as it was demonstrated for the IVn/gtt conformer of glycine,[20] which is characterized by a low-energy barrier for its relaxation toward the most stable Ip/ttt conformer.[105] Moreover, the generation of a large amount of *Tt*-PA (up to 75% of the total conformational mixture) recently demonstrated by means of a NIR-induced excitation of the OH overtone of *Tc*-PA, opens up new possible pathways for the detection of *Ct*-PA in low-temperature matrices. According to our investigation, TS(*C-T*) (imaginary frequency of *i*39 cm^{-1}) is obtained by the rotation of the carboxylic group (O5−C3−C2−O1 dihedral angle) by about 110 deg, whereas all the other structural parameters are essentially unchanged with respect to the *Tt*-PA conformer. Considering *Tt*-PA as a starting point, either the excitation of the *Tt*-PA C3−C2 torsion overtones or UV induced rotamerization might lead to the creation of *Ct*-PA. These experiments can be performed in different cryogenic matrices, thus allowing for enhanced stabilization effects.[29,125]

3.2. Rotational Spectra of PA Conformers. Table 7 collects the rotational parameters and the vibrationally corrected dipole moment components for the three conformers investigated. All conformers contain one methyl group with a low torsional barrier (estimated as 336−390 cm^{-1} for *Tc*-PA[122,165]), thus resulting in a splitting of the vibrational ground state in the A and E-symmetry sublevels, as pointed out by Kisiel et al. in ref 122 for *Tc*-PA. Computationally, the derived set of rotational constants are

DOI: 10.1021/acs.jctc.5b00580
J. Chem. Theory Comput. XXXX, XXX, XXX−XXX

Table 7. Rotational Parameters[a] of the *Tc*-, *Tt*-, and *Ct*-Pyruvic Acid Conformers

	Tc-PA			*Tt*-PA			*Ct*-PA		
parameter	B2PLYP/AVTZ	best theo[b]	Exp.[c]	B2PLYP/AVTZ	best theo[b]	scaled[d]	B2PLYP/AVTZ	best theo[b]	scaled[d]
A_0/MHz	5506.31	5537.68	5535.46113(18)	5601.93	5638.10	5636.61	5528.35	5561.05	5559.58
B_0/MHz	3556.56	3586.68	3583.408634(78)	3448.05	3476.34	3473.34	3444.83	3477.49	3474.49
C_0/MHz	2189.86	2206.23	2204.858443(63)	2167.27	2183.61	2182.38	2161.99	2178.43	2177.21
Δ_J/kHz	0.678	0.684	0.675114(35)	0.599	0.606	0.598	0.595	0.597	0.589
Δ_{JK}/kHz	−0.814	−0.843	−0.77911(12)	−0.538	−0.575	−0.531	−0.449	−0.458	−0.424
Δ_K/kHz	1.499	1.546	1.49373(49)	1.393	1.445	1.397	1.299	1.318	1.274
δ_J/kHz	0.266	0.269	0.264241(16	0.230	0.233	0.229	0.228	0.230	0.226
δ_K/kHz	0.548	0.565	0.552491(97)	0.582	0.598	0.585	0.570	0.587	0.574
Φ_J/mHz	0.146	0.146	0.1239(86)	0.144	0.146	.	0.109	0.111	.
Φ_{JK}/mHz	−0.363	−0.327	[0.0]	0.148	0.104	.	4.649	3.138	.
Φ_{KJ}/mHz	−2.009	−2.090	−1.71(13)	−4.452	−4.207	.	−25.762	−18.746	.
Φ_K/mHz	3.006	3.054	5.61(48)	4.826	4.612	.	21.460	15.939	.
ϕ_J/mHz	0.113	0.113	0.0718(46)	0.112	0.112	.	0.099	0.099	.
ϕ_{JK}/mHz	0.422	0.387	[0.0]	0.661	0.588	.	1.825	1.435	.
ϕ_K/mHz	2.714	2.706	2.441(76)	5.527	5.167	.	27.223	19.912	.
$\mu_a^{298\ K}$/D	2.35	2.38	2.27(2)[e]	−0.29	−0.36		−0.23	−0.14	
$\mu_b^{298\ K}$/D	−0.19	−0.16	0.35(2)[e]	1.25	1.26		3.68	3.79	
$\mu_c^{298\ K}$/D	0.00	0.00		0.00	0.00		0.00	0.00	

[a]Watson *A*-reduction. [b]Best-estimated equilibrium rotational and quartic centrifugal-distortion constants and dipole moment components. For rotational constants and dipole moment components, the best-estimated equilibrium constants are augmented by vibrational corrections from hybrid "best cheap"/B2PLYP force fields. Sextic centrifugal-distortion constants are obtained from hybrid "best cheap"/B2PLYP force fields. See text. [c]From the simultaneous fit of A and E-symmetry transitions with ERHAM code from ref 122. [d]Scaled rotational parameters from eq 9. Sextic centrifugal-distortion constants were not scaled because of the limited experimental accuracy. Scaled B2PLYP/aug-cc-pVTZ rotational constants (in MHz): for the *Tt*-PA: A_0 = 5631.58, B_0 = 3474.08, and C_0 = 2182.11; for *Ct*-PA: A_0 = 5557.62, B_0 = 3470.84, and C_0 = 2176.80. [e]ref.:[168] absolute values.

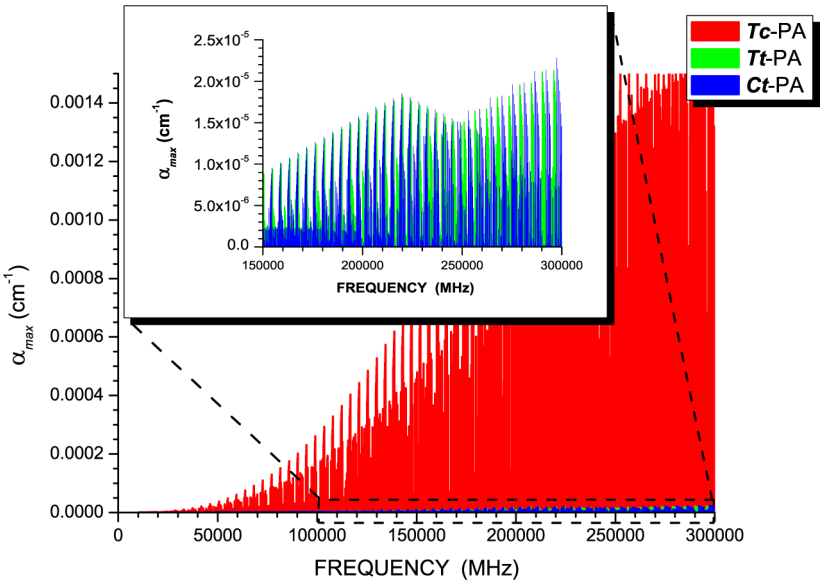

Figure 2. Simulation of the stick rotational spectra (in the 0−300 GHz frequency range) of *Tc*-, *Tt*-, and *Ct*-PA based on experimental spectroscopic parameters for *Tc*-PA and on scaled parameters for *Tt*- and *Ct*-PA. In the inset, the rotational spectra of the latter two conformers are better shown.

those of an unperturbed vibrational ground state. For comparison purposes, the best-estimated and B2PLYP/aug-cc-pVTZ parameters are reported in Table 7. We note that they agree with one another well within 1% for what concerns the rotational constants. The larger differences (a few percents) observed for the quartic centrifugal-distortion constants are mostly due to the small absolute values of these parameters.

For the *Tc*-PA conformer, the experimental rotational parameters obtained in ref 122 from the simultaneous fit of A and E-symmetry transitions are also given in Table 7. This set of constants was chosen because it is considered to reproduce well those of an unperturbed state. The comparison of these values with best estimates allows us to address the expected accuracy of our computations. We note that for the rotational constants, the agreement is very good, with discrepancies smaller than 0.1% (for B2PLYP/aug-cc-pVTZ, the discrepancies are about one order of magnitude larger), while for the quartic centrifugal-distortion constants, the differences increase to a few percents (in this case the differences for

DOI: 10.1021/acs.jctc.5b00580
J. Chem. Theory Comput. XXXX, XXX, XXX−XXX

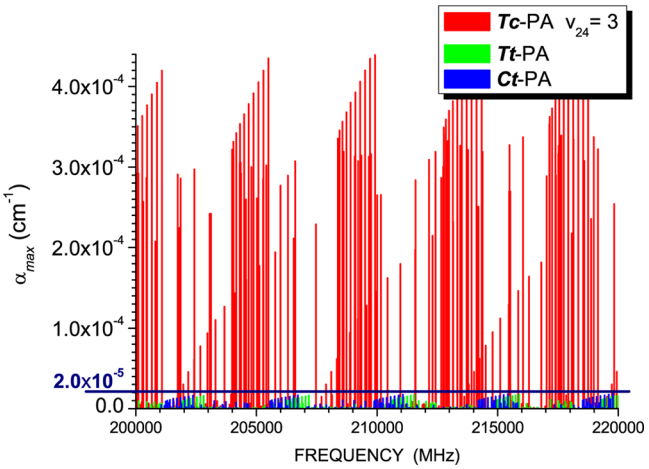

Figure 3. Simulation of the stick rotational spectra in the 200−220 GHz frequency range of *Tc*-PA in its ν_{24} = 3 vibrational state and of *Tt*- and *Ct*-PA in their vibrational ground state based on experimental spectroscopic parameters for the former conformer and on scaled parameters for *Tt*- and *Ct*-PA.

B2PLYP/aug-cc-pVTZ are smaller). To further improve the theoretical predictions for the *Tt*- and *Ct*-PA conformers, an empirical scaling procedure was employed. For a generic spectroscopic parameter *X*, the scaling is performed using the expression

$$X^{t}_{\mathrm{scal}} = X^{t}_{\mathrm{calc}} \times (X^{Tc}_{\mathrm{exp}}/X^{Tc}_{\mathrm{calc}}) \quad (9)$$

where the superscript *t* corresponds to either *Tt*-PA or *Ct*-PA, while *Tc* refers to the most abundant conformer. In eq 9, scal, exp, and calc denote the scaled, experimental, and quantum-chemically calculated values for *X*, respectively. It can be noted that such a scaling procedure leads to very similar results for the rotational constants when considering either the best theoretical estimates or the B2PLYP/aug-cc-pVTZ ones as starting points.

The spectroscopic parameters of Table 7 were used to simulate the rotational spectra for all conformers. An example is provided by Figure 2, which depicts the comparison of the rotational spectra of *Tc*-, *Tt*-, and *Ct*-PA in the 0−300 GHz frequency range at 328 K, as obtained using the experimental data for *Tc*-PA and the scaled constants eq 9 for the other two conformers. The line intensities account for the different population ratio, based on the values reported in Table 6. In the simulation of the spectra only the transitions with a peak absorption coefficient, α_{max} (cm^{-1}), greater than 6.8 × 10^{-6} cm^{-1} and with $J \leq 50$ have been considered. From Figure 2, it is evident that the rotational spectrum is dominated by the *Tc*-PA conformer, with the rotational spectra of *Tt*- and *Ct*-PA being ∼80−90 times less intense. These spectra are even less intense than those observed and assigned by Kisiel et al.[122] for the vibrational states ν_{23} = 1 and ν_{24} = 1,2,3 of the major conformer. Figure 3 shows how the line intensities of the rotational spectra of *Tt*- and *Ct*-PA in their vibrational ground

Table 8. Theoretical Harmonic Vibrational Wavenumbers (cm^{-1}) of the *Tc*-, *Tt*-, and *Ct*-Pyruvic Acid Conformers

			Tc-PA			*Tt*-PA			*Ct*-PA		
mode	sym.	assignment[a]	B2PLYP/AVTZ	CCSD(T)/VTZ	"best cheap"[b]	B2PLYP/AVTZ	CCSD(T)/VTZ	"best cheap"[b]	B2PLYP/AVTZ	CCSD(T)/VTZ	"best cheap"[b]
1	A′	ν(OH)	3631	3667	3662	3744	3770	3759	3737	3766	3753
2	A′	ν(CH_3) as	3181	3174	3177	3180	3171	3175	3175	3168	3171
3	A′	ν(CH_3) s	3066	3056	3054	3066	3056	3054	3064	3053	3052
4	A′	ν(C3═O)	1820	1853	1829	1780	1812	1789	1814	1842	1827
5	A′	ν(C2═O)	1754	1773	1766	1777	1793	1785	1783	1797	1792
6	A′	δ(CH_3) as	1468	1464	1468	1471	1466	1471	1475	1470	1475
7	A′	ν(C−C) as	1413	1430	1418	1411	1427	1418	1404	1397	1406
8	A′	δ(CH_3) s	1384	1394	1389	1384	1389	1393	1346	1372	1357
9	A′	δ(COH)	1253	1271	1260	1226	1241	1236	1197	1207	1207
10	A′	ν(C−O)	1159	1166	1163	1143	1150	1150	1131	1145	1143
11	A′	γ(CH_3)	987	984	989	978	976	983	987	984	992
12	A′	ν(C−C)s	769	775	775	743	750	752	735	731	732
13	A′	δ(C2═O)	609	608	607	594	590	596	611	608	614
14	A′	δ(C3═O)	527	532	528	516	521	519	483	483	485
15	A′	δ (CCO)	392	395	391	389	387	389	400	399	401
16	A′	δ(CCC)	252	253	249	249	247	247	256	254	257
17	A″	ν(CH_3) as	3127	3126	3126	3128	3126	3126	3127	3124	3125
18	A″	δ(CH_3) as	1474	1470	1474	1478	1473	1477	1483	1477	1482
19	A″	γ(CH_3)	1047	1040	1047	1048	1041	1047	1051	1041	1050
20	A″	γ(C3═O)	744	741	732	735	733	733	733	741	743
21	A″	τ(OH)	707	701	704	625	620	616	621	613	616
22	A″	γ(C2═O)	397	394	393	382	380	378	386	382	383
23	A″	τ(CH_3)	125	124	129	132	132	139	158	157	163
24	A″	τ(C−C)	93	94	95	38	44	39	20	22	22
		MAE[c]	5.5	5.0		5.4	4.8		5.4	5.0	
		|MAX|[c]	31	24		15	23		16	15	

[a]Approximate description: ν-stretching, δ-bending, γ-rocking, τ-torsion. [b]Best-estimated "best cheap" harmonic vibrational wavenumbers. [c]Mean absolute error (MAE) and maximum absolute deviations (|MAX|) with respect to the best-estimates "best cheap".

DOI: 10.1021/acs.jctc.5b00580
J. Chem. Theory Comput. XXXX, XXX, XXX−XXX

Table 9. Theoretical Anharmonic Vibrational Wavenumbers (cm^{-1}) and IR Intensities (km mol^{-1}) of *Tc*-Pyruvic Acid[a]

		observed		B2PLYP/AVTZ		"best cheap"/B2PLYP[b]	
final state[c]	assignment[c]	Ar[d]	gas[e]	ν	I	ν	I
1^2		6630	6696	6657	2.63	6737	2.55
1 + 4		5228.3		5211	0.22	5256	0.22
1 + 7		4819.7	4851	4807	0.36	4847	0.36
1 + 8		4795.4		4771	1.92	4810	1.89
1 + 12 + 14			4729	4696	0.37	4743	0.37
$1 + 13^2$		4643.7		4631	0.08	4664	0.05
1 + 9		4631.8	4668	4624	2.25	4666	2.21
1 + 10		4565.9	4589	4550	1.02	4592	1.02
1 + 20 + 22		4540.7		4555	0.27	4565	0.25
2 + 7			4418	4416	0.23	4413	0.23
1 + 12		4194.4		4178	0.25	4224	0.24
1 + 20		4158.8	4200	4161	0.43	4180	0.42
1 + 21		4119.3	4145	4118	0.34	4148	0.33
1 + 13		4037.5		4031	0.18	4065	0.18
2 + 11		4000		4008	0.19	4004	0.19
1 + 15		3818.5		3811	0.89	3845	0.88
4^2		3584.2		3552	6.05	3570	1.18
1	ν(OH)	3432	3463	3430	106.43	3465	111.25
4 + 7			3199	3161	0.18	3175	0.18
2	$\nu(CH_3)$ as	3032.3	3025	3041	4.49	3035	4.68
17	$\nu(CH_3)$ as	2982		2985	0.71	2984	0.67
3	$\nu(CH_3)$ s	2936	2941	2955	0.51	2948	0.54
5 + 11		2725		2685	0.68	2700	0.67
6 + 9		2642		2634	0.07	2642	0.07
8 + 9		2565		2537	0.93	2549	0.88
7 + 10		2515	2515	2496	1.25	2511	1.23
10^2			2268	2243	0.54	2259	0.54
9 + 11		2178		2174	0.26	2183	0.25
12 + 20 + 21		2119		2127	0.19	2128	0.21
4 + 16		2062		2039	0.34	2045	0.35
9 + 12		1957.2	1966	1954	0.25	1972	0.23
10 + 12		1891		1871	0.33	1890	0.32
9 + 153		1804.7		1810	4.81	1816	5.53
4	ν(C3═O)	1799.5	1804	1785	205.38	1794	208.39
11 + 12 + 24		1797.6		1809	0.37	1818	0.20
15 + 19 + 22		1795.7		1785	0.27	1792	0.27
9 + 14		1730.2		1725	13.91	1734	16.63
5	ν(C2═O)	1728.8	1737	1720	27.64	1732	13.41
10 + 13		1727.9		1723	17.09	1730	42.63
6	$\delta(CH_3)$ as	1423.7	1424	1436	13.59	1436	3.47
18	$\delta(CH_3)$ as	1408.3		1431	6.25	1430	8.27
7	ν(C−C) as	1384.5	1391	1382	126.36	1385	43.51
8	$\delta(CH_3)$ s	1354.6	1360	1361	136.84	1364	109.50
12 + 14		1290.3	1296	1267	25.29	1279	25.45
9	δ(COH)	1214.4	1211	1207	117.83	1214	121.59
10	ν(C−O)	1136.8	1133	1130	19.25	1132	48.83
19	$\gamma(CH_3)$	1017.8	1030	1022	1.61	1022	1.61
11	$\gamma(CH_3)$	968.4	970	969	21.31	971	21.14
12	ν(C−C)s	762.2	761	750	7.77	756	6.19
20	γ (C3═O)	678.8		720	0.62	702	1.43
21	τ(OH)	664.2	668	675	96.59	673	114.78
13	δ (C2═O)	603.8	604	601	15.70	600	15.69
14	δ (C3═O)	534.9		527	1.67	527	1.98
22	γ (C2═O)		394	394	16.22	390	16.08
15	δ (CCO)		389	384	8.53	383	8.53
16	δ(CCC)		258	257	22.98	253	23.81
23	$\tau(CH_3)$		134	117	0.41	111	1.13
24	τ(C−C)		90	91	7.51	89	7.00
ALL[f]	MAE			19.7		8.8	

DOI: 10.1021/acs.jctc.5b00580
J. Chem. Theory Comput. XXXX, XXX, XXX−XXX

Table 9. continued

final state[c]	assignment[c]	observed		B2PLYP/AVTZ		"best cheap"/B2PLYP[b]	
		Ar[d]	gas[e]	ν	I	ν	I
	|MAX|			54		41	
FUND[g]	MAE			10.4		7.4	
	|MAX|			36		24	
Comb+Over[h]	MAE			26.5		9.7	
	|MAX|			54		41	

[a]Fundamental transitions, overtones, and combination bands up to the 3-quanta are compared with available experimental results. [b]Hybrid "best cheap"/B2PLYP force field. [c]Final state n^i (n-normal mode, i-quanta), approximate description: ν-stretching, δ-bending, γ-rocking, τ-torsion. [d]Ar-Matrix results from refs 29 and 119. [e]Gas-phase results below 1000 cm^{-1} from ref 23; gas-phase results above 1000 cm^{-1} from ref 124. [f]Mean absolute error (MAE) and maximum absolute deviations (|MAX|) with respect to experiment evaluated for all reported bands. Experimental gas-phase data were used as references when available; experimental results from Ar-Matrix were corrected for a matrix effect (red shift of 30 cm^{-1} for one quanta of ν(OH)), see text for the details. [g]Mean absolute error (MAE) and maximum absolute deviations (|MAX|) with respect to experiment evaluated for fundamental transitions. [h]Mean absolute error (MAE) and maximum absolute deviations (|MAX|) with respect to experiment evaluated for overtones and combinational bands.

state compare with those of *Tc*-PA in the ν_{24} = 3 state for a small frequency range (200−220 GHz). It is observed that the spectra of *Tt*- and *Ct*-PA are about 20 times less intense. The conclusion is that due to the overall congestion of the rotational spectrum of pyruvic acid and to the small intensity of their transitions, the *Tt*- and *Ct*-PA conformers are hardly characterizable by means of experiments in the field of rotational spectroscopy. Such a conclusion further points out the importance of the present accurate computational study.

Since the experimental observation of the rotational spectra of *Tt*- and *Ct*-PA is very challenging, albeit not entirely impossible and with the chances improved by increasing the temperature (for instance, at T = 340 K the population ratio is 89.6:8.8:1.6), it is important to discuss the accuracy of our predictions based on scaled spectroscopic parameters. The scaling procedure is an approach extensively used in the field of rotational spectroscopy, and its validity has been discussed, for example, in refs 166 and 167. On the basis of our previous experience, this scaling is expected to reduce the discrepancies with respect to experiment to less than 0.01% for rotational constants and on average to less than 2.0% for the quartic centrifugal-distortion terms. Based on the available experimental results for *Tc*-PA (refs 121, 122, and 168), our best-estimated computed parameters provide predictions with a relative mean accuracy of about 0.05% in the 0−300 GHz frequency range. A rotational frequency of 100 GHz is therefore predicted with an accuracy of 50 MHz. For the same frequency, the relative error is expected to decrease to 0.005−0.01% when applying the scaling procedure, thus resulting in discrepancies of 5−10 MHz for our prediction.

3.3. Spectroscopic IR Signatures of Observed and Elusive PA Conformers. The harmonic frequencies of *Tc*-, *Tt*-, and *Ct*-PA computed at the B2PLYP/aug-cc-pVTZ and CCSD(T)/cc-pVTZ levels of theory are compared to their "best cheap" counterparts in Table 8. For all conformers, B2PLYP/aug-cc-pVTZ and CCSD(T)/cc-pVTZ show similar deviations from the best theoretical estimates with MAEs of about 5 cm^{-1}. The largest discrepancy (about 30 cm^{-1}) is observed for the ν(OH) mode of *Tc*-PA, which is involved in an intramolecular hydrogen bond. This effect can be attributed to the enhanced accuracy requirements for the description of the PES along hydrogen bonds,[169] with similar results obtained also at the B2PLYP-D3/aug-cc-pVTZ level. For all other modes and conformers, B2PLYP/aug-cc-pVTZ harmonic frequencies show maximum absolute deviations with respect to the "best cheap" ones smaller than those issuing from the much more expensive CCSD(T)/cc-pVTZ computations. Moreover, the OH stretching frequencies show systematic errors that can be strongly reduced by a linear regression (*vide infra*). These results further confirm the good performance of the B2PLYP/aug-cc-pVTZ computational model.

Recent experimental results for the *Tc*- and *Tt*-PA conformers from Ar Matrix[29] complemented by gas-phase[124] measurements allow us to assess the accuracy of vibrational wavenumbers computed at the B2PLYP/aug-cc-pVTZ level and by means of the hybrid "best cheap"/B2PLYP model. Tables 9 and 10 list the anharmonic vibrational frequencies for fundamental transitions, overtones, and combination bands, up to about 7000 cm^{-1}, along with their corresponding anharmonic IR intensities.

For *Tc*-PA, in most cases the present results confirm the assignments from a previous study based on B3LYP/6-311+G(d,p) anharmonic computations with IR anharmonic intensities up to two-quanta transitions.[29] However, the improved description of the PES and the availability of intensities for three-quanta transitions also permitted some reassignments. For instance, the *Tc*-PA band at 4540.7 cm^{-1}, tentatively assigned to the $2\nu_4+\nu_{11}$ combination, has been reassigned to a combination involving the OH-stretching ($\nu_1+\nu_{20}+\nu_{22}$) once the IR intensities for 3-quanta transitions were also considered. Moreover, some of the combinations previously assigned to 2-quanta transitions (i.e., the bands at 4643.7, 1797.6, and 1795.7 cm^{-1}) have been reassigned to 3-quanta combinations. The results from the present work allowed us to also revise tentative assignments of the gas-phase spectra,[124] thus leading to the full characterization of all fundamental bands and of more than 30 nonfundamental transitions up to 7000 cm^{-1}. The MAE and maximum absolute deviations (|MAX|) with respect to experiment were evaluated for all reported bands, considering whenever possible experimental gas-phase data as reference. The comparison of the gas-phase and Ar-Matrix results points out that all transitions involving the OH-stretching mode are affected by a matrix-induced red shift of the order of 30 cm^{-1} per quantum of ν(OH). For the error analysis, this correction has been applied to all experimental bands observed in Ar Matrix that have been assigned to fundamentals, overtones, and combinations involving ν(OH). In the case of fundamental transitions, the B2PLYP/aug-cc-pVTZ level shows a MAE of about 10 cm^{-1}, while the hybrid "best cheap"/B2PLYP model improves the MAE to 7.5 cm^{-1} and

DOI: 10.1021/acs.jctc.5b00580
J. Chem. Theory Comput. XXXX, XXX, XXX−XXX

Table 10. Theoretical Anharmonic Vibrational Wavenumbers (cm^{-1}) and IR Intensities (km mol^{-1}) of *Tt*-Pyruvic Acid[a]

		observed		B2PLYP/AVTZ		"best cheap"/B2PLYP[b]	
final state[c]	assignment[c]	Ar[d]	gas[e]	ν	I	ν	I
1^2		6944	6975	6953	4.16	6990	4.10
1 + 4		5325.5		5305	0.41	5332	0.41
1 + 5		5316		5303	0.35	5329	0.35
1 + 7		4934		4930	0.16	4953	0.16
1 + 8		4907.2		4892	0.71	4917	0.70
1 + 9		4750.3		4729	0.40	4756	0.39
3 + 4		4702.5		4699	0.05	4701	0.05
1 + 10		4670.6		4668	0.19	4691	0.18
2 + 6		4441.1		4453	0.52	4449	0.52
2 + 7		4400.2		4408	0.27	4406	0.22
17 + 18		4400.2		4401	0.22	4405	0.27
3 + 18		4381		4384	0.14	4377	0.14
8 + 17		4329.8		4325	0.10	4332	0.10
1 + 20		4288		4280	0.14	4307	0.14
1 + 21		4143.7		4150	0.95	4156	0.96
1	ν(OH)	3556.2	3579	3559	72.30	3575	72.46
4 + 5		3504.3		3479	3.96	3499	3.90
5^2		3484		3471	2.69	3491	2.58
2	$\nu(CH_3)$ as	3030.4		3034	2.87	3030	4.74
17	$\nu(CH_3)$ as	2982.4		2984	2.25	2983	2.28
3	$\nu(CH_3)$ s			2953	0.02	2945	0.01
5 + 10		2878		2854	1.03	2871	1.02
7 + 10		2496		2481	1.07	2495	1.05
$4 + 1^2$		1818.6		1790	3.65	1804	3.05
4	ν(C3═O)	1763.7		1747	10.41	1757	10.83
7 + 15		1761.4		1758	1.21	1764	1.32
5	ν(C2═O)	1750.8		1745	329.58	1755	319.41
12 + 19		1749.4		1741	14.11	1736	27.44
18	$\delta(CH_3)$ as	1426.1		1432	8.99	1432	8.35
6	$\delta(CH_3)$ as	1422.3		1428	7.48	1427	5.83
7	ν(C−C) as	1387		1375	2.71	1381	3.45
8	$\delta(CH_3)$ s	1356.9		1356	36.39	1362	32.01
9	δ(COH)	1205		1192	15.78	1198	16.41
10	ν(C−O)	1118.8		1111	227.94	1118	229.17
15 + 20		1116.6		1105	1.59	1114	2.26
19	$\gamma(CH_3)$	1019.3		1024	1.36	1022	1.35
11	$\gamma(CH_3)$	961.9		958	45.84	962	38.79
20	γ (C3═O)	722.7		724	9.40	730	4.61
12	ν(C−C)s	716.4		719	26.46	716	27.54
13	δ (C2═O)	592.1		587	72.69	589	72.67
21	τ(OH)	588.2		594	82.07	587	87.80
14	δ (C3═O)			515	1.78	517	1.79
15	δ (CCO)			385	1.03	384	1.00
22	γ (C2═O)			374	0.08	370	0.06
16	δ(CCC)			249	9.23	241	8.38
23	$\tau(CH_3)$			104	0.00	102	0.00
24	τ(C−C)			22	6.08	24	6.24
ALL[f]	MAE			13.9		5.9	
	|MAX|			44		17	
FUND[g]	MAE			6.4		3.6	
	|MAX|			20		7	
Comb+Over[h]	MAE			19.4		7.6	
	|MAX|			44		17	

[a]Fundamental transitions, overtones and combination bands up to the 3-quanta are compared with available experimental results. [b]Hybrid "best cheap"/B2PLYP force field. [c]Final state n^i (n-normal mode, i-quanta), approximate description: ν-stretching, δ-bending, γ-rocking, τ-torsion. [d]Ar-Matrix results from refs 29 and 119. [e]Gas-phase results from ref 124. [f]Mean absolute error (MAE) and maximum absolute deviations (|MAX|) with respect to experiment evaluated for all reported bands. Experimental gas-phase data were used as references when available, experimental results from Ar Matrix has been corrected for a matrix effect (red shift of 23 cm^{-1} for one quanta of ν(OH)), see text for the details. [g]Mean absolute error (MAE) and maximum absolute deviations (|MAX|) with respect to experiment evaluated for fundamental transitions. [h]Mean absolute error (MAE) and maximum absolute deviations (|MAX|) with respect to experiment evaluated for overtones and combinational bands.

DOI: 10.1021/acs.jctc.5b00580
J. Chem. Theory Comput. XXXX, XXX, XXX−XXX

Table 11. Theoretical Anharmonic Vibrational Wavenumbers (cm^{-1}) and IR Intensities (km mol^{-1}) of *Ct*-Pyruvic Acid in the Spectra Region up to the 7000 cm^{-1}[a]

		B2PLYP/AVTZ		"best cheap"/ B2PLYP[b]	
final state[c]	assignment[c]	ν	I	ν	I
1^2		6941.0	4.22	6981.8	4.16
1	ν(OH)	3553.2	63.12	3571.3	63.32
2	$\nu(CH_3)$ as	3029.5	5.13	3027.5	6.48
17	$\nu(CH_3)$ as	2983.3	2.84	2981.4	2.84
3	$\nu(CH_3)$ s	2951.6	0.03	2946.7	0.21
4	ν(C3═O)	1780.9	149.56	1794.4	145.25
9 + 13		1756.9	15.55	1770.5	21.65
5	ν(C2═O)	1749.2	150.90	1759.3	163.27
11 + 14		1448.2	8.53	1454.1	4.55
18	$\delta(CH_3)$ as	1440.2	8.85	1440.3	8.25
6	$\delta(CH_3)$ as	1436.2	8.29	1437.7	16.19
7	$\delta(CH_3)$ s	1368.0	34.85	1369.4	34.63
8	ν(C−C) as	1335.8	20.89	1341.4	19.14
13 + 20		1319.1	3.97	1330.7	6.43
14 + 20		1192.0	14.71	1203.3	11.92
21^2		1184.8	11.93	1183.9	20.16
9	δ(COH)	1155.6	53.28	1165.6	56.60
15 + 20		1111.6	22.37	1122.8	21.77
10	ν(C−O)	1102.2	126.58	1111.1	201.37
12 + 22		1089.0	17.65	1088.5	12.92
11 + 24^2		1022.5	82.62	1031.3	57.76
19	$\gamma(CH_3)$	1025.6	1.43	1024.5	1.43
11	$\gamma(CH_3)$	969.2	20.94	980.2	11.08
21 + 22		980.1	2.26	970.1	12.09
20	γ(C3═O)	716.2	7.71	725.6	7.69
12	ν(C−C)s	714.2	35.42	712.1	37.00
13	δ(C2═O)	604.1	35.33	607.4	35.37
21	τ(OH)	598.7	86.64	596.1	85.34
14	δ(C3═O)	473.9	8.42	476.2	8.41
15	δ(CCO)	398.1	3.41	400.0	3.39
22	γ(C2═O)	381.4	0.06	378.9	0.03
16	δ(CCC)	255.6	1.17	256.7	1.17
23	$\tau(CH_3)$	161.0	0.03	158.4	0.03
24	τ(C−C)	25.5	0.28	26.9	0.28

[a]All fundamental transitions along with overtones and combination bands up to the 3-quanta with IR intensities greater than 4 km mol^{-1} are reported. [b]Hybrid "best cheap"/B2PLYP force field. [c]Final state n^i (n-normal mode, i-quanta), approximate description: ν-stretching, δ-bending, γ-rocking, τ-torsion.

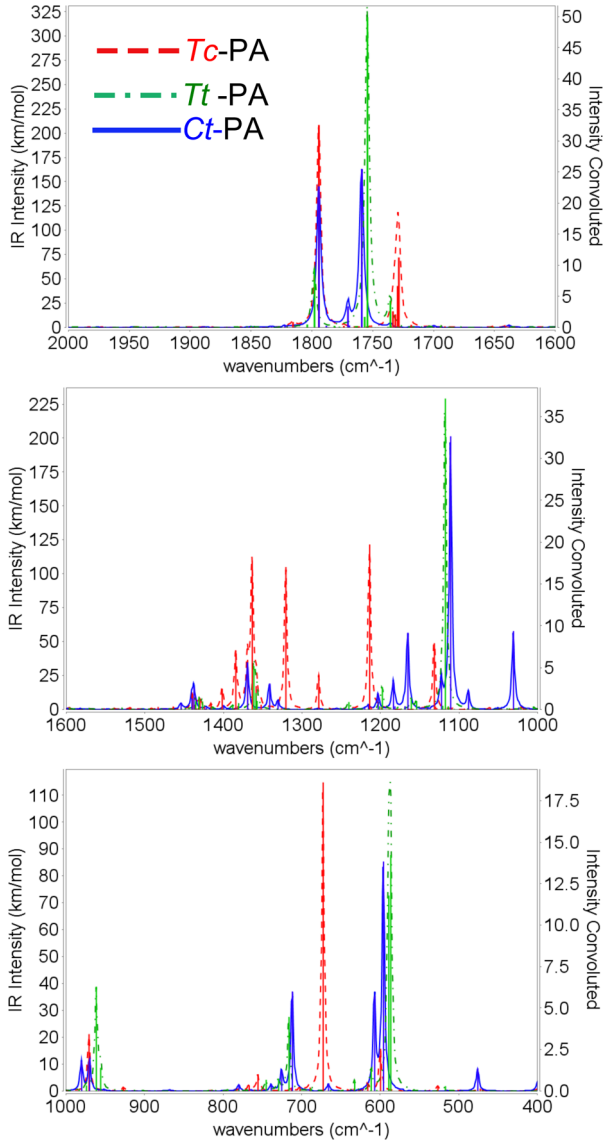

Figure 4. Anharmonic IR spectra of the *Tc*-, *Tt*-, and *Ct*-pyruvic acid conformers in the 400−1000 cm^{-1}, 1000−1600 cm^{-1}, and 1600−2000 cm^{-1} ranges computed with the hybrid "best cheap"/B2PLYP scheme. Stick-spectra (IR intensities in km mol^{-1}) and spectra line shapes convoluted with Lorentzian distribution functions with a HWHM of 2 cm^{-1} are presented.

furthermore lowers the maximum discrepancy by about 10 cm^{-1}. Slightly larger differences between the two sets of data are observed for nonfundamental transitions, thus leading to a total MAE of about 20 cm^{-1} for B2PLYP/aug-cc-pVTZ and less than 10 cm^{-1} for the best theoretical estimates. However, as already noted, the lower accuracy of the B2PLYP/aug-cc-pVTZ results can be attributed to the harmonic value for the ν(OH) mode. In fact, the MAE computed for all transitions not involving ν(OH) decreases to about 13 cm^{-1}. This finding is important in view of investigating larger systems, since it suggests that improvements of the harmonic part of the PES beyond B2PLYP/aug-cc-pVTZ can be obtained by using reduced-dimensionality models.[170] As an alternative, it is possible to correct the B2PLYP/aug-cc-pVTZ ν(OH) value by scaling the harmonic frequency. To take into account hydrogen-bonding effects, a linear dependence of the scaling factor is considered, and it was found that the correction $\omega_{Corr} = 0.9\omega_{B2PLYP}+392$ leads to a remarkable agreement (2 cm^{-1}) with "best cheap" values for all conformers. We note that such a correction cannot be obtained by uniform scaling factors, which however might be systematically applied to improve 'well behaving' frequencies.[171]

For the *Tt*-PA conformer, most of the experimental transitions were observed in Ar Matrix, as in the case of the most recent experiment by Reva et al.,[29] where this conformer was effectively produced by NIR-pumping. The only available gas-phase results are related to ν(OH) and its overtones that, owing to the lack of an intramolecular hydrogen bond, are observed at higher wavenumbers than those of *Tc*-PA and show smaller matrix effects. A matrix-induced red-shift of 23 cm^{-1} has been estimated for one quantum of ν(OH), and such a correction has been applied in the statistical analysis for all transitions involving the OH-

DOI: 10.1021/acs.jctc.5b00580
J. Chem. Theory Comput. XXXX, XXX, XXX−XXX

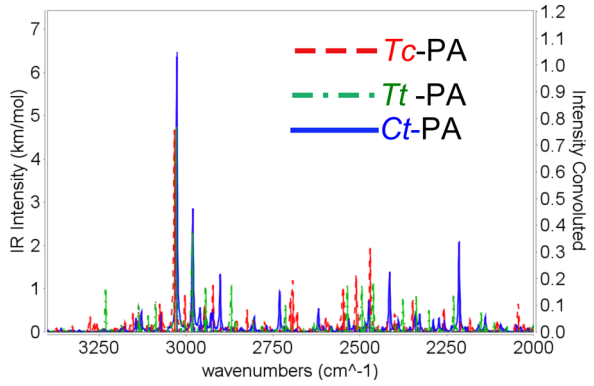

Figure 5. Anharmonic IR spectra of the *Tc*-, *Tt*-, and *Ct*-pyruvic acid conformers in the 2000−3400 cm^{-1} range (related to the overtones and combination bands) computed with the hybrid "best cheap"/B2PLYP scheme. Stick-spectra (IR intensities in km mol^{-1}) and spectra line shapes convoluted with Lorentzian distribution functions with a HWHM of 2 cm^{-1} are presented.

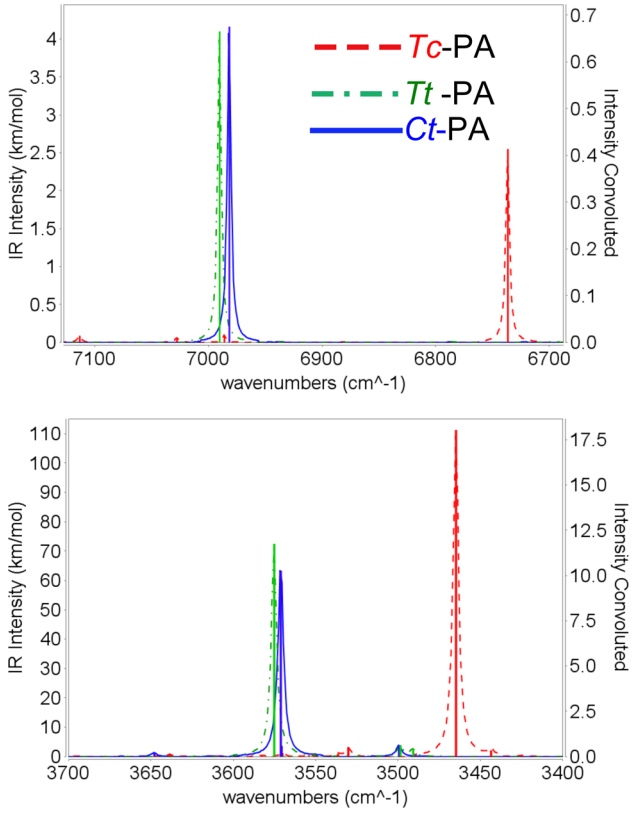

Figure 6. Anharmonic IR spectra of the *Tc*-, *Tt*-, and *Ct*-pyruvic acid conformers in the 3400−3700 cm^{-1} and 6700−7100 cm^{-1} ranges (related to the ν(OH) and its overtones) computed with the hybrid "best cheap"/B2PLYP scheme. Stick-spectra (IR intensities in km mol^{-1}) and spectra line shapes convoluted with Lorentzian distribution functions with a HWHM of 2 cm^{-1} are presented.

stretching mode. For most transitions, the assignment by Reva et al. has been confirmed, while reassignments for the bands at 1116.6, 1749.4, 1761.4, 1818.6, and 2496 cm^{-1}, along with some NIR transitions, are also proposed. In particular, in a previous work[119] the band at 1116.6 cm^{-1} was tentatively assigned to the low intensity ν_{19} fundamental, which is predicted at 1022 cm^{-1} by our computations. A reanalysis of the experimental spectra of ref 29 shows indeed a low intensity band at 1019.3 cm^{-1}, which we assign to ν_{19}, whereas the band at 1116.3 cm^{-1} has been reassigned to the $\nu_{15}+\nu_{20}$ combination, predicted at 1114 cm^{-1} and more intense than the ν_{19} fundamental. Concerning the reliability of our theoretical results, the differences between the two computational models are again larger than the average for the modes involving ν(OH), and also in this case they can be traced back to the harmonic part of the force field. More importantly, both models show a very good accuracy with a MAE below 7 cm^{-1} for the fundamental transitions. For the best theoretical estimates, the MAE remains smaller than 7 cm^{-1} and the maximum discrepancy does not exceed 17 cm^{-1}, when also considering nonfundamental bands. The overall accuracy of both computational models, i.e., a MAE of about 7−10 cm^{-1} for B2PLYP/aug-cc-pVTZ and 4−7 cm^{-1} for "best cheap"/B2PLYP, is in line with previous observations.[49] In particular, the best estimates of the "difficult" ν(OH) fundamental transitions agree with gas-phase results within the experimental error (4 cm^{-1}) for both observed conformers.

The very good agreement between the best-estimated IR spectra of the *Tc*- and *Tt*-PA conformers with their experimental counterparts allows us to accurately predict the IR spectra of the yet-unobserved *Ct*-PA conformer in view of its possible detection via *ad hoc* experiments. All fundamental and the most intense nonfundamental transitions computed at the B2PLYP/aug-cc-pVTZ and "best cheap"/B2PLYP levels are listed in Table 11, with the latter model considered able to provide predictions with an accuracy of about ±5 cm^{-1}. The comparison between the anharmonic spectra of the three pyruvic acid conformers is graphically presented in Figures 4, 5, and 6, in order to provide further insights on the best spectrum ranges or transitions to be considered characteristic for the *Ct*-PA conformer. Starting from the most intense transitions, in the 1700−1800 cm^{-1} spectrum range related to the C═O stretchings, one can note that the *Ct*-PA bands overlap with either the *Tc*-PA or *Tt*-PA ones. The situation is similar also for the OH-stretching, since in this case *Ct*-PA and *Tt*-PA show very similar spectrum features for both fundamental and overtones (see Figure 6). Moreover, as expected, the 2000−3400 cm^{-1} spectrum range (depicted in Figure 5) is rather congested showing many low-intensity transitions for each conformer. However, in the spectrum range between 400 and 1600 cm^{-1} a few characteristic transitions, which can be considered as "fingerprints" of *Ct*-PA, can be observed (see Figure 4). The most evident bands lie at 476, 1031, and 1166 cm^{-1}, which correspond to the ν_{14} (C═O bending), the combination $\nu_{11}+2\nu_{24}$ and ν_9 (COH bending) bands, respectively. In particular, the rather intense ν_9 fundamental is predicted to be shifted by more than 30 cm^{-1} from the corresponding transitions of the *Tt*-PA and *Tc*-PA conformers and also does not show intense close-lying nonfundamental transitions.

4. CONCLUDING REMARKS

In the present work we have analyzed the structures, relative stabilities, rotational, and vibrational spectra of the three lowest energy conformers of pyruvic acid (PA) by means of a state-of-the-art quantum-mechanical approach including anharmonic contributions. The proposed computational strategy employs CCSD(T) evaluations of energies, geometries, and harmonic force fields extrapolated to the complete basis set limit and also including core−valence correlation contributions. On top of these computations, anharmonic effects of

DOI: 10.1021/acs.jctc.5b00580
J. Chem. Theory Comput. XXXX, XXX, XXX−XXX

both mechanical and electrical origin are evaluated at the B2PLYP/aug-cc-pVTZ level. All these results are finally employed in the framework of the generalized second-order perturbation theory (GVPT2) approach to evaluate the thermodynamic and spectroscopic parameters required to the theoretical support of state-of-the-art experimental studies.

Starting from the determination of the first semiexperimental structure for the most stable conformer, we provide accurate estimates for the structures and relative stabilities of the other two low-lying energy minima with an accuracy of 0.001 Å, 0.1 deg, and 1 kJ mol^{-1} for bond lengths, angles, and free energies, respectively. At the same time, computed vibrational frequencies agree with their experimental counterparts well within a 10 cm^{-1} error bar, and the computed infrared intensities lead to simulated spectra matching all the main experimental features within the mid-IR and NIR spectral ranges, thus allowing to disentangle the contributions of low-intensity fundamentals from those of high-intensity overtones and combination bands.

We have also validated the accuracy of a low-cost computational model based exclusively on density functional theory. The impressive performance of new double hybrid functionals (here B2PLYP), whose reliability can be further enhanced by adding dispersion correction (D3) for energies and/or by using a "template-molecule" approach for bond lengths and a scaling factor for the OH stretching harmonic frequencies, has been pointed out.

In more general terms, the present study confirms that state-of-the-art quantum-mechanical computations beyond the harmonic approximation, and accounting for the leading anharmonic effects for both small and large amplitude motions, represent an invaluable complement to the most sophisticated experimental approaches toward the comprehensive and accurate characterization of flexible systems with multiple low-energy minima in terms of both thermodynamic quantities and spectroscopic signatures.

■ ASSOCIATED CONTENT

Supporting Information

The Supporting Information is available free of charge on the ACS Publications website at DOI: 10.1021/acs.jctc.5b00580.

Cartesian coordinates of the structures of the five stationary points optimized at the B2PLYP/aug-cc-pVTZ level together with those of the *Tc*, *Tt*, and *Ct* conformers evaluated by means of the "best CC" composite scheme (PDF)

■ AUTHOR INFORMATION

Corresponding Author

*E-mail: vincenzo.barone@sns.it.

Notes

The authors declare no competing financial interest.

■ ACKNOWLEDGMENTS

The research leading to these results has received funding from the European Union's Seventh Framework Programme (FP7/2007-2013) under the grant agreement No. ERC-2012-AdG-320951-DREAMS. This work was supported by Italian MIUR (PRIN 2012 "STAR: Spectroscopic and computational Techniques for Astrophysical and atmospheric Research" and PON 1078) and by the University of Bologna (RFO funds). The high performance computer facilities of the DREAMS center (http://dreams.sns.it) are acknowledged for providing computer resources. C.P. and M.B. also acknowledge the COST CMTS-Action CM1405 (MOLIM: MOLecules In Motion). Prof. Rui Fausto and Dr. Igor Reva are acknowledged for fruitful discussions and for providing the experimental data of their IR spectroscopic measurements on pyruvic acid.

■ REFERENCES

(1) Robertson, E. G.; Simons, J. P. Getting Into Shape: Conformational and Supramolecular Landscapes in Small Biomolecules and their Hydrated Clusters. *Phys. Chem. Chem. Phys.* **2001**, *3*, 1−18.

(2) Chin, W.; Piuzzi, F.; Dimicoli, I.; Mons, M. Probing the Competition Between Secondary Structures and Local Preferences in Gas Phase Isolated Peptide Backbones. *Phys. Chem. Chem. Phys.* **2006**, *8*, 1033−1048.

(3) Zwier, T. S. Laser Probes of Conformational Isomerization in Flexible Molecules and Complexes. *J. Phys. Chem. A* **2006**, *110*, 4133−4150.

(4) de Vries, M. S.; Hobza, P. Gas-phase Spectroscopy of Biomolecular Building Blocks. *Annu. Rev. Phys. Chem.* **2007**, *58*, 585−612.

(5) Caminati, W. Nucleic Acid Bases in the Gas Phase. *Angew. Chem., Int. Ed.* **2009**, *48*, 9030−9033.

(6) Steber, A. L.; Neill, J. L.; Zaleski, D. P.; Pate, B. H.; Lesarri, A.; Bird, R. G.; Vaquero-Vara, V.; Pratt, D. W. Structural Studies of Biomolecules in the Gas Phase by Chirped-pulse Fourier Transform Microwave Spectroscopy. *Faraday Discuss.* **2011**, *150*, 227−242.

(7) Becucci, M.; Pietraperzia, G. In *Computational Strategies for Spectroscopy: from Small Molecules to Nano Systems*; Barone, V., Ed.; John Wiley & Sons, Inc.: 2011; Chapter Quest for Accurate Models: Some Challenges from Gas-Phase Experiments on Medium-Size Molecules and Clusters, pp 25−35.

(8) Fausto, R.; Khriachtchev, L.; Hamm, P. In *Physics and Chemistry at Low Temperatures*; Khriachtchev, L., Ed.; Pan Stanford Publishing Pte. Ltd.: Singapore, 2011.

(9) Puzzarini, C.; Biczysko, M. In *Structure Elucidation in Organic Chemistry*; Cid, M. M., Bravo, J., Eds.; Wiley-VCH Verlag GmbH & Co. KGaA: 2015; Chapter Computational Spectroscopy Tools for Molecular Structure Analysis, pp 27−64.

(10) Alonso, J. L.; López, J. C. *Microwave Spectroscopy of Biomolecular Building Blocks*; Topics in Current Chemistry; Springer: Berlin, Heidelberg, 2015; pp 1−67.

(11) Häber, T.; Seefeld, K.; Engler, G.; Grimme, S.; Kleinermanns, K. IR/UV Spectra and Quantum Chemical Calculations of Trp-Ser: Stacking Interactions Between Backbone and Indole Side-chain. *Phys. Chem. Chem. Phys.* **2008**, *10*, 2844−2851.

(12) Baquero, E. E.; James, W. H.; Choi, S. H.; Gellman, S. H.; Zwier, T. S. Single-Conformation Ultraviolet and Infrared Spectroscopy of Model Synthetic Foldamers:β-Peptides Ac-β^3-hPhe-β^3-hAla-NHMe and Ac-β^3-hAla-β^3-hPhe-NHMe. *J. Am. Chem. Soc.* **2008**, *130*, 4795−4807.

(13) Albrieux, F.; Calvo, F.; Chirot, F.; Vorobyev, A.; Tsybin, Y. O.; Lepere, V.; Antoine, R.; Lemoine, J.; Dugourd, P. Conformation of Polyalanine and Polyglycine Dications in the Gas Phase: Insight from Ion Mobility Spectrometry and Replica-Exchange Molecular Dynamics. *J. Phys. Chem. A* **2010**, *114*, 6888−6896.

(14) Garand, E.; Kamrath, M. Z.; Jordan, P. A.; Wolk, A. B.; Leavitt, C. M.; McCoy, A. B.; Miller, S. J.; Johnson, M. A. Determination of Noncovalent Docking by Infrared Spectroscopy of Cold Gas-Phase Complexes. *Science* **2012**, *335*, 694−698.

(15) Dean, J. C.; Buchanan, E. G.; Zwier, T. S. Mixed 14/16 Helices in the Gas Phase: Conformation-Specific Spectroscopy of Z-$(Gly)_n$, n = 1, 3, 5. *J. Am. Chem. Soc.* **2012**, *134*, 17186−17201.

(16) Cabezas, C.; Peña, M. I.; López, J. C.; Alonso, J. L. Seven Conformers of Neutral Dopamine Revealed in the Gas Phase. *J. Phys. Chem. Lett.* **2013**, *4*, 486−490.

(17) Puzzarini, C.; Biczysko, M.; Barone, V.; Largo, L.; Peña, I.; Cabezas, C.; Alonso, J. L. Accurate Characterization of the Peptide Linkage in the Gas Phase: a Joint Quantum-chemical and Rotational Spectroscopy Study of the Glycine Dipeptide Analogue. *J. Phys. Chem. Lett.* **2014**, *5*, 534−540.
(18) Peña, I.; Cabezas, C.; Alonso, J. L. The Nucleoside Uridine Isolated in the Gas Phase. *Angew. Chem., Int. Ed.* **2015**, *54*, 2991−2994.
(19) Bazso, G.; Magyarfalvi, G.; Tarczay, G. Near-infrared Laser Induced Conformational Change and UV Laser Photolysis of Glycine in Low-temperature Matrices: Observation of a Short-lived Conformer. *J. Mol. Struct.* **2012**, *1025*, 33−42.
(20) Balabin, R. M. Conformational Equilibrium in Glycine: Experimental Jet-Cooled Raman Spectrum. *J. Phys. Chem. Lett.* **2010**, *1*, 20−23.
(21) Lapinski, L.; Reva, I.; Nowak, M. J.; Fausto, R. Five Isomers of Monomeric Cytosine and their Interconversions Induced by Tunable UV Laser Light. *Phys. Chem. Chem. Phys.* **2011**, *13*, 9676−9684.
(22) Nunes, C. M.; Lapinski, L.; Fausto, R.; Reva, I. Near-IR Laser Generation of a High-energy Conformer of L-alanine and the Mechanism of its Decay in a Low-temperature Nitrogen Matrix. *J. Chem. Phys.* **2013**, *138*, 125101.
(23) Bazsó, G.; Najbauer, E. E.; Magyarfalvi, G.; Tarczay, G. Near-Infrared Laser Induced Conformational Change of Alanine in Low-Temperature Matrixes and the Tunneling Lifetime of Its Conformer VI. *J. Phys. Chem. A* **2013**, *117*, 1952−1962.
(24) Kuş, N.; Sharma, A.; Peña, I.; Bermúdez, M. C.; Cabezas, C.; Alonso, J. L.; Fausto, R. Conformers of β-aminoisobutyric Acid Probed by Jet-cooled Microwave and Matrix Isolation Infrared Spectroscopic Techniques. *J. Chem. Phys.* **2013**, *138*, 144305.
(25) Najbauer, E. E.; Bazsó, G.; Gbi, S.; Magyarfalvi, G.; Tarczay, G. Exploring the Conformational Space of Cysteine by Matrix Isolation Spectroscopy Combined with Near-Infrared Laser Induced Conformational Change. *J. Phys. Chem. B* **2014**, *118*, 2093−2103.
(26) Olbert-Majkut, A.; Lundell, J.; Wierzejewska, M. Light-Induced Opening and Closing of the Intramolecular Hydrogen Bond in Glyoxylic Acid. *J. Phys. Chem. A* **2014**, *118*, 350−357.
(27) Olbert-Majkut, A.; Wierzejewska, M.; Lundell, J. Light-induced, Site-selective Isomerization of Glyoxylic Acid in Solid Xenon. *Chem. Phys. Lett.* **2014**, *616*−*617*, 91−97.
(28) Khriachtchev, L. Matrix-Isolation Studies of Non-Covalent Interactions: More Sophisticated Approaches. *J. Phys. Chem. A* **2015**, *119*, 2735−2746.
(29) Reva, I.; Nunes, C. M.; Biczysko, M.; Fausto, R. Conformational Switching in Pyruvic Acid Isolated in Ar and N_2 Matrixes: Spectroscopic Analysis, Anharmonic Simulation, and Tunneling. *J. Phys. Chem. A* **2015**, *119*, 2614−2627.
(30) Puzzarini, C.; Biczysko, M.; Barone, V.; Pena, I.; Cabezas, C.; Alonso, J. L. Accurate Molecular Structure and Spectroscopic Properties of Nucleobases: a Combined Computational-microwave Investigation of 2-thiouracil as a Case Study. *Phys. Chem. Chem. Phys.* **2013**, *15*, 16965−16975.
(31) Puzzarini, C.; Ali, A.; Biczysko, M.; Barone, V. Accurate Spectroscopic Characterization of Protonated Oxirane: A Potential Prebiotic Species in Titan's Atmosphere. *Astrophys. J.* **2014**, *792*, 118.
(32) Barone, V.; Biczysko, M.; Puzzarini, C. Quantum Chemistry Meets Spectroscopy for Astrochemistry: Increasing Complexity toward Prebiotic Molecules. *Acc. Chem. Res.* **2015**, *48*, 1413−1422.
(33) Barone, V.; Biczysko, M.; Bloino, J. Fully Anharmonic IR and Raman Spectra of Medium-size Molecular Systems: Accuracy and Interpretation. *Phys. Chem. Chem. Phys.* **2014**, *16*, 1759−1787.
(34) Pettersson, M.; Lundell, J.; Khriachtchev, L.; Räsänen, M. IR Spectrum of the Other Rotamer of Formic Acid, cis-HCOOH. *J. Am. Chem. Soc.* **1997**, *119*, 11715−11716.
(35) *Equilibrium Molecular Structures: From Spectroscopy to Quantum Chemistry*; Demaison, J., Boggs, J. E., Császár, A. G., Eds.; CRC Press, Taylor & Francis Group: 2011.
(36) Puzzarini, C.; Stanton, J. F.; Gauss, J. Quantum-chemical Calculation of Spectroscopic Parameters for Rotational Spectroscopy. *Int. Rev. Phys. Chem.* **2010**, *29*, 273−367.
(37) Puzzarini, C. In *Computational Strategies for Spectroscopy, from Small Molecules to Nano Systems*; Barone, V., Ed.; John Wiley & Sons, Inc.: 2011; Chapter Computational Approach to Rotational Spectroscopy, pp 261−307.
(38) Puzzarini, C. Rotational spectroscopy meets theory. *Phys. Chem. Chem. Phys.* **2013**, *15*, 6595−6607.
(39) Puzzarini, C.; Cazzoli, G.; López, J. C.; Alonso, J. L.; Baldacci, A.; Baldan, A.; Stopkowicz, S.; Cheng, L.; Gauss, J. Rotational Spectra of Rare Isotopic Species of Fluoroiodomethane: Determination of the Equilibrium Structure from Rotational Spectroscopy and Quantum-chemical Calculations. *J. Chem. Phys.* **2012**, *137*, 024310.
(40) Raghavachari, K.; Trucks, G. W.; Pople, J. A.; Head-Gordon, M. A Fifth-order Perturbation Comparison of Electron Correlation Theories. *Chem. Phys. Lett.* **1989**, *157*, 479−483.
(41) Heckert, M.; Kállay, M.; Tew, D. P.; Klopper, W.; Gauss, J. Basis-set Extrapolation Techniques for the Accurate Calculation of Molecular Equilibrium Geometries Using Coupled-Cluster Theory. *J. Chem. Phys.* **2006**, *125*, 044108.
(42) Heckert, M.; Kállay, M.; Gauss, J. Molecular Equilibrium Geometries Based on Coupled-Cluster Calculations Including Quadruple Excitations. *Mol. Phys.* **2005**, *103*, 2109−2115.
(43) Tew, D. P.; Klopper, W.; Heckert, M.; Gauss, J. Basis Set Limit CCSD(T) Harmonic Vibrational Frequencies. *J. Phys. Chem. A* **2007**, *111*, 11242−11248.
(44) Biczysko, M.; Panek, P.; Scalmani, G.; Bloino, J.; Barone, V. Harmonic and Anharmonic Vibrational Frequency Calculations with the Double-Hybrid B2PLYP Method: Analytic Second Derivatives and Benchmark Studies. *J. Chem. Theory Comput.* **2010**, *6*, 2115−2125.
(45) Becke, A. D. Density-functional Thermochemistry. III. The Role of Exact Exchange. *J. Chem. Phys.* **1993**, *98*, 5648−5652.
(46) Grimme, S. Semiempirical Hybrid Density Functional with Perturbative Second-order Correlation. *J. Chem. Phys.* **2006**, *124*, 034108.
(47) Puzzarini, C.; Biczysko, M. Microsolvation of 2-Thiouracil: Molecular Structure and Spectroscopic Parameters of the Thiouracil-Water Complex. *J. Phys. Chem. A* **2015**, *119*, 5386−5395.
(48) Biczysko, M.; Bloino, J.; Brancato, G.; Cacelli, I.; Cappelli, C.; Ferretti, A.; Lami, A.; Monti, S.; Pedone, A.; Prampolini, G.; Puzzarini, C.; Santoro, F.; Trani, F.; Villani, G. Integrated Computational Approaches for Spectroscopic Studies of Molecular Systems in the Gas Phase and in Solution: Pyrimidine as a Test Case. *Theor. Chem. Acc.* **2012**, *131*, 1201/1−19.
(49) Barone, V.; Biczysko, M.; Bloino, J.; Puzzarini, C. Accurate Molecular Structures and Infrared Spectra of trans-2,3-dideuterooxirane, Methyloxirane, and trans-2,3-dimethyloxirane. *J. Chem. Phys.* **2014**, *141*, 034107/1−17.
(50) Kozuch, S.; Martin, J. M. L. Spin-component-scaled Double Hybrids: An Extensive Search for the Best Fifth-rung Functionals Blending DFT and Perturbation Theory. *J. Comput. Chem.* **2013**, *34*, 2327−2344.
(51) Chan, B.; Goerigk, L.; Radom, L. On the Inclusion of post-MP2 Contributions to Double-Hybrid Density Functionals. *J. Comput. Chem.* **2015**, DOI: 10.1002/jcc.23972.
(52) Carnimeo, I.; Puzzarini, C.; Tasinato, N.; Stoppa, P.; Charmet, A. P.; Biczysko, M.; Cappelli, C.; Barone, V. Anharmonic Theoretical Simulations of Infrared Spectra of Halogenated Organic Compounds. *J. Chem. Phys.* **2013**, *139*, 074310.
(53) Pesonen, J., Halonen, L. *Adv. Chem. Phys.*; John Wiley & Sons, Inc.: 2003; Vol. *125*, Chapter Recent Advances in the Theory of Vibration-Rotation Hamiltonians, pp 269−349.
(54) Császár, A. G.; Fabri, C.; Szidarovszky, T.; Matyus, E.; Furtenbacher, T.; Czako, G. The Fourth Age of Quantum Chemistry: Molecules in Motion. *Phys. Chem. Chem. Phys.* **2012**, *14*, 1085−1106.

DOI: 10.1021/acs.jctc.5b00580
J. Chem. Theory Comput. XXXX, XXX, XXX−XXX

(55) Yagi, K.; Taketsugu, T.; Hirao, K.; Gordon, M. S. Direct Vibrational Self-consistent Field Method: Applications to H_2O and H_2CO. *J. Chem. Phys.* **2000**, *113*, 1005−1017.
(56) Norris, L. S.; Ratner, M. A.; Roitberg, A. E.; Gerber, R. B. Møller-Plesset Perturbation Theory Applied to Vibrational Problems. *J. Chem. Phys.* **1996**, *105*, 11261−11267.
(57) Chaban, G. M.; Jung, J. O.; Gerber, R. B. Ab initio Calculation of Anharmonic Vibrational States of Polyatomic Systems: Electronic Structure Combined with Vibrational Self-consistent Field. *J. Chem. Phys.* **1999**, *111*, 1823−1829.
(58) Carter, S.; Culik, S. J.; Bowman, J. M. Vibrational Self-consistent Field Method for Many-mode Systems: A New Approach and Application to the Vibrations of CO Adsorbed on Cu(100). *J. Chem. Phys.* **1997**, *107*, 10548−10469.
(59) Bowman, J. M. Beyond Platonic Molecules. *Science* **2000**, *290*, 724−725.
(60) Bowman, J. M.; Carter, S.; Huang, X. MULTIMODE: A Code to Calculate Rovibrational Energies of Polyatomic Molecules. *Int. Rev. Phys. Chem.* **2003**, *22*, 533−549.
(61) Carter, S.; Handy, N. The Vibrations of H_2O_2, Studied by "Multimode", with a Large Amplitude Motion. *J. Chem. Phys.* **2000**, *113*, 987−993.
(62) Rauhut, G.; Hrenar, T. A Combined Variational and Perturbational Study on the Vibrational Spectrum of P_2F_4. *Chem. Phys.* **2008**, *346*, 160−166.
(63) Carter, S.; Sharma, A. R.; Bowman, J. M.; Rosmus, P.; Tarroni, R. Calculations of Rovibrational Energies and Dipole Transition Intensities for Polyatomic Molecules Using MULTIMODE. *J. Chem. Phys.* **2009**, *131*, 224106.
(64) Heislbetz, S.; Rauhut, G. Vibrational Multiconfiguration Self-consistent Field Theory: Implementation and Test Calculations. *J. Chem. Phys.* **2010**, *132*, 124102.
(65) Christiansen, O. Møller-Plesset Perturbation Theory for Vibrational Wave Functions. *J. Chem. Phys.* **2003**, *119*, 5773−5781.
(66) Christiansen, O. Vibrational Structure Theory: New Vibrational Wave Function Methods for Calculation of Anharmonic Vibrational Energies and Vibrational Contributions to Molecular Properties. *Phys. Chem. Chem. Phys.* **2007**, *9*, 2942−2953.
(67) Christiansen, O. Selected New Developments in Vibrational Structure Theory: Potential Construction and Vibrational Wave Function Calculations. *Phys. Chem. Chem. Phys.* **2012**, *14*, 6672−6687.
(68) Roy, T. K.; Gerber, R. B. Vibrational Self-Consistent Field Calculations for Spectroscopy of Biological Molecules: New Algorithmic Developments and Applications. *Phys. Chem. Chem. Phys.* **2013**, *15*, 9468−9492.
(69) Nielsen, H. H. The Vibration-Rotation Energies of Molecules. *Rev. Mod. Phys.* **1951**, *23*, 90−136.
(70) Mills, I. M. In *Molecular Spectroscopy: Modern Research*; Rao, K. N., Mathews, C. W., Eds.; Academic Press: New York, 1972; Chapter Vibration-Rotation Structure in Asymmetric- and Symmetric-Top Molecules, pp 115−140.
(71) Truhlar, D. G.; Olson, R. W.; Jeannotte, A. C.; Overend, J. Anharmonic Force Constants of Polyatomic Molecules. Test of the Procedure for Deducing a Force Field from the Vibration-rotation Spectrum. *J. Am. Chem. Soc.* **1976**, *98*, 2373−2379.
(72) Isaacson, A. D.; Truhlar, D. G.; Scanlon, K.; Overend, J. Tests of Approximation Schemes for Vibrational Energy Levels and Partition Functions for Triatomics: H_2O and SO_2. *J. Chem. Phys.* **1981**, *75*, 3017−3024.
(73) Clabo, D. A., Jr.; Allen, W. D.; Remington, R. B.; Yamaguchi, Y.; Schaefer, H. F., III A Systematic Study of Molecular Vibrational Anharmonicity and Vibration-rotation Interaction by Self-consistent-fied Higher-derivative Methods. Asymmetric Top Molecules. *Chem. Phys.* **1988**, *123*, 187−239.
(74) Allen, W. D.; Yamaguchi, Y.; Császár, A. G.; Clabo, D. A., Jr.; Remington, R. B.; Schaefer, H. F., III A Systematic Study of Molecular Vibrational Anharmonicity and Vibration-rotation Interaction by Self-consistent-fied Higher-derivative Methods. Linear Polyatomic Molecules. *Chem. Phys.* **1990**, *145*, 427−466.
(75) Amos, R. D.; Handy, N. C.; Green, W. H.; Jayatilaka, D.; Willetts, A.; Palmieri, P. Anharmonic Vibrational Properties of CH_2F_2: A Comparison of Theory and Experiment. *J. Chem. Phys.* **1991**, *95*, 8323−8336.
(76) Maslen, P. E.; Handy, N. C.; Amos, R. D.; Jayatilaka, D. Higher Analytic Derivatives. IV. Anharmonic Effects in the Benzene Spectrum. *J. Chem. Phys.* **1992**, *97*, 4233−4254.
(77) Gaw, F.; Willetts, A.; Handy, N.; Green, W. In *Advances in Molecular Vibrations and Collision Dynamics*; Bowman, J. M., Ed.; JAI Press: 1991; Vol. *1B*, pp 169−185.
(78) Zhang, Q.; Day, P. N.; Truhlar, D. G. The Accuracy of Second Order Perturbation Theory for Multiply Excited Vibrational Energy Levels and Partition Functions for a Symmetric Top Molecular Ion. *J. Chem. Phys.* **1993**, *98*, 4948−4958.
(79) Barone, V. Characterization of the Potential Energy Surface of the HO_2 Molecular System by a Density Functional Approach. *J. Chem. Phys.* **1994**, *101*, 10666−10676.
(80) Barone, V. Anharmonic Vibrational Properties by a Fully Automated Second-order Perturbative Approach. *J. Chem. Phys.* **2005**, *122*, 014108.
(81) Barone, V. Vibrational Zero-point Energies and Thermodynamic Functions Beyond the Harmonic Approximation. *J. Chem. Phys.* **2004**, *120*, 3059−3065.
(82) Martin, J. M. L.; Lee, T. J.; Taylor, P. M.; François, J.-P. The Anharmonic Force Field of Ethylene, C_2H_4, by Means of Accurate ab initio Calculations. *J. Chem. Phys.* **1995**, *103*, 2589−2602.
(83) Dressler, S.; Thiel, W. Anharmonic Force Fields from Density Functional Theory. *Chem. Phys. Lett.* **1997**, *273*, 71−78.
(84) Stanton, J. F.; Gauss, J. Anharmonicity in the Ring Stretching Modes of Diborane. *J. Chem. Phys.* **1998**, *108*, 9218−9220.
(85) Ruud, K.; Åstrand, P.-O.; Taylor, P. R. An Efficient Approach for Calculating Vibrational Wave Functions and Zero-point Vibrational Corrections to Molecular Properties of Polyatomic Molecules. *J. Chem. Phys.* **2000**, *112*, 2668−2683.
(86) Ruden, T. A.; Taylor, P. R.; Helgaker, T. Automated Calculation of Fundamental Frequencies: Application to AlH_3 using the Coupled-Cluster Singles-and-Doubles with Perturbative Triples Method. *J. Chem. Phys.* **2003**, *119*, 1951−1960.
(87) Stanton, J. F.; Gauss, J. Analytic Second Derivatives in High-order Many-Body Perturbation and Coupled-Cluster Theories: Computational Considerations and Applications. *Int. Rev. Phys. Chem.* **2000**, *19*, 61−95.
(88) Neugebauer, J.; Hess, B. A. Fundamental Vibrational Frequencies of Small Polyatomic Molecules from Density-functional Calculations and Vibrational Perturbation Theory. *J. Chem. Phys.* **2003**, *118*, 7215−7225.
(89) Vázquez, J.; Stanton, J. F. Simple(r) Algebraic Equation for Transition Moments of Fundamental Transitions in Vibrational Second-order Perturbation Theory. *Mol. Phys.* **2006**, *104*, 377−388.
(90) Vázquez, J.; Stanton, J. F. Treatment of Fermi Resonance Effects on Transition Moments in Vibrational Perturbation Theory. *Mol. Phys.* **2007**, *105*, 101−109.
(91) Barone, V.; Bloino, J.; Guido, C. A.; Lipparini, F. A Fully Automated Implementation of VPT2 Infrared Intensities. *Chem. Phys. Lett.* **2010**, *496*, 157−161.
(92) Krasnoshchekov, S. V.; Isayeva, E. V.; Stepanov, N. F. Numerical-Analytic Implementation of the Higher-Order Canonical Van Vleck Perturbation Theory for the Interpretation of Medium-Sized Molecule Vibrational Spectra. *J. Phys. Chem. A* **2012**, *116*, 3691−3709.
(93) Bloino, J.; Biczysko, M.; Barone, V. General Perturbative Approach for Spectroscopy, Thermodynamics, and Kinetics: Methodological Background and Benchmark Studies. *J. Chem. Theory Comput.* **2012**, *8*, 1015−1036.
(94) Bloino, J.; Barone, V. A Second-order Perturbation Theory Route to Vibrational Averages and Transition Properties of Molecules: General Formulation and Application to Infrared and

DOI: 10.1021/acs.jctc.5b00580
J. Chem. Theory Comput. XXXX, XXX, XXX−XXX

Vibrational Circular Dichroism Spectroscopies. *J. Chem. Phys.* **2012**, *136*, 124108.
(95) Hermes, M. R.; Hirata, S. Second-order Many-body Perturbation Expansions of Vibrational Dyson Self-energies. *J. Chem. Phys.* **2013**, *139*, 034111.
(96) Rosnik, A. M.; Polik, W. F. VPT2+K Spectroscopic Constants and Matrix Elements of the Transformed Vibrational Hamiltonian of a Polyatomic Molecule with Resonances using Van Vleck Perturbation Theory. *Mol. Phys.* **2014**, *112*, 261−300.
(97) Krasnoshchekov, S. V.; Isayeva, E. V.; Stepanov, N. F. Criteria for First- and Second-order Vibrational Resonances and Correct Evaluation of the Darling-Dennison Resonance Coefficients Using the Canonical Van Vleck Perturbation Theory. *J. Chem. Phys.* **2014**, *141*, 234114.
(98) Krasnoshchekov, S. V.; Stepanov, N. F. Nonempirical Anharmonic Vibrational Perturbation Theory Applied to Biomolecules: Free-Base Porphin. *J. Phys. Chem. A* **2015**, *119*, 1616−1627.
(99) Bloino, J. A VPT2 Route to Near-Infrared Spectroscopy: The Role of Mechanical and Electrical Anharmonicity. *J. Phys. Chem. A* **2015**, *119*, 5269−5287.
(100) Piccardo, M.; Bloino, J.; Barone, V. Generalized Vibrational Perturbation Theory for Rotovibrational Energies of Linear, Symmetric and Asymmetric Tops: Theory, Approximations and Automated Approaches to Deal with Medium-to-Large Molecular Systems. *Int. J. Quantum Chem.* **2015**, *115*, 948−982.
(101) Barone, V.; Biczysko, M.; Bloino, J.; Borkowska-Panek, M.; Carnimeo, I.; Panek, P. Toward Anharmonic Computations of Vibrational Spectra for Large Molecular Systems. *Int. J. Quantum Chem.* **2012**, *112*, 2185−2200.
(102) Biczysko, M.; Bloino, J.; Carnimeo, I.; Panek, P.; Barone, V. Fully ab initio IR Spectra for Complex Molecular Systems from Perturbative Vibrational Approaches: Glycine as a Test Case. *J. Mol. Struct.* **2012**, *1009*, 74−82.
(103) Barone, V.; Biczysko, M.; Bloino, J.; Puzzarini, C. Glycine Conformers: a Never-ending Story? *Phys. Chem. Chem. Phys.* **2013**, *15*, 1358−1363.
(104) Barone, V.; Biczysko, M.; Bloino, J.; Puzzarini, C. Characterization of the Elusive Conformers of Glycine from State-of-the-Art Structural, Thermodynamic, and Spectroscopic Computations: Theory Complements Experiment. *J. Chem. Theory Comput.* **2013**, *9*, 1533−1547.
(105) Barone, V.; Biczysko, M.; Bloino, J.; Puzzarini, C. The Performance of Composite Schemes and Hybrid CC/DFT Model in Predicting Structure, Thermodynamic and Spectroscopic Parameters: the Challenge of the Conformational Equilibrium in Glycine. *Phys. Chem. Chem. Phys.* **2013**, *15*, 10094−10111.
(106) Puzzarini, C.; Penocchio, E.; Biczysko, M.; Barone, V. Molecular Structure and Spectroscopic Signatures of Acrolein: Theory Meets Experiment. *J. Phys. Chem. A* **2014**, *118*, 6648−6656.
(107) Latouche, C.; Barone, V. Computational Chemistry Meets Experiments for Explaining the Behavior of Bibenzyl: A Thermochemical and Spectroscopic (Infrared, Raman, and NMR) Investigation. *J. Chem. Theory Comput.* **2014**, *10*, 5586−5592.
(108) Barone, V.; Baiardi, A.; Biczysko, M.; Bloino, J.; Cappelli, C.; Lipparini, F. Implementation and Validation of a Multi-purpose Virtual Spectrometer for Large Systems in Complex Environments. *Phys. Chem. Chem. Phys.* **2012**, *14*, 12404−12422.
(109) Barone, V.; Baiardi, A.; Bloino, J. New Developments of a Multifrequency Virtual Spectrometer: Stereo-Electronic, Dynamical, and Environmental Effects on Chiroptical Spectra. *Chirality* **2014**, *26*, 588−600.
(110) Barone, V.; Bloino, J.; Biczysko, M.; Santoro, F. Fully Integrated Approach to Compute Vibrationally Resolved Optical Spectra: From Small Molecules to Macrosystems. *J. Chem. Theory Comput.* **2009**, *5*, 540−554.
(111) Bloino, J.; Biczysko, M.; Santoro, F.; Barone, V. General Approach to Compute Vibrationally Resolved One-Photon Electronic Spectra. *J. Chem. Theory Comput.* **2010**, *6*, 1256−1274.
(112) Baiardi, A.; Bloino, J.; Barone, V. General Time Dependent Approach to Vibronic Spectroscopy Including Franck-Condon, Herzberg-Teller, and Duschinsky Effects. *J. Chem. Theory Comput.* **2013**, *9*, 4097−4115.
(113) Baiardi, A.; Bloino, J.; Barone, V. A General Time-dependent Route to Resonance-Raman Spectroscopy Including Franck-Condon, Herzberg-Teller and Duschinsky Effects. *J. Chem. Phys.* **2014**, *141*, 114108.
(114) Licari, D.; Baiardi, A.; Biczysko, M.; Egidi, F.; Latouche, C.; Barone, V. Implementation of a Graphical User Interface for the Virtual Multifrequency Spectrometer: The VMS-Draw Tool. *J. Comput. Chem.* **2015**, *36*, 321−334.
(115) Christofk, H. R.; van der Heiden, M. G.; Harris, M. H.; Ramanathan, A.; Gerszten, R. E.; Wei, R.; Fleming, M. D.; Schreiber, S. L.; Cantley, L. C. The M2 Splice Isoform of Pyruvate Kinase Is Important for Cancer Metabolism and Tumour Growth. *Nature* **2008**, *452*, 230−233.
(116) Li, Y.; Chen, J.; Lun, S.-Y. Biotechnological Production of Pyruvic Acid. *Appl. Microbiol. Biotechnol.* **2001**, *57*, 451−459.
(117) Vaida, V. Spectroscopy of Photoreactive Systems: Implications for Atmospheric Chemistry. *J. Phys. Chem. A* **2009**, *113*, 5−18.
(118) Jardine, K. J.; Sommer, E. D.; Saleska, S. R.; Huxman, T. E.; Harley, P. C.; Abrell, L. Gas Phase Measurements of Pyruvic Acid and Its Volatile Metabolites. *Environ. Sci. Technol.* **2010**, *44*, 2454−2460.
(119) Reva, I. D.; Stepanian, S. G.; Adamowicz, L.; Fausto, R. Combined FTIR Matrix Isolation and Ab Initio Studies of Pyruvic Acid: Proof for Existence of the Second Conformer. *J. Phys. Chem. A* **2001**, *105*, 4773−4780.
(120) Murto, J.; Raaska, T.; Kunttu, H.; Räsänen, M. Conformers and Vibrational Spectra of Pyruvic Acid: an Ab Initio Study. *J. Mol. Struct.: THEOCHEM* **1989**, *200*, 93−101.
(121) Dyllick-Brenzinger, C.; Bauder, A.; Gunthard, H. The Substitution Structure, Barrier to Internal Rotation, and Low Frequency Vibrations of Pyruvic Acid. *Chem. Phys.* **1977**, *23*, 195−206.
(122) Kisiel, Z.; Pszczolkowski, L.; Bialkowska-Jaworska, E.; Charnley, S. B. The Millimeter Wave Rotational Spectrum of Pyruvic Acid. *J. Mol. Spectrosc.* **2007**, *241*, 220−229.
(123) Pulay, P.; Meyer, W.; Boggs, J. E. Cubic Force Constants and Equilibrium Geometry of Methane from Hartree-Fock and Correlated Wavefunctions. *J. Chem. Phys.* **1978**, *68*, 5077−5085.
(124) Plath, K. L.; Takahashi, K.; Skodje, R. T.; Vaida, V. Fundamental and Overtone Vibrational Spectra of Gas-Phase Pyruvic Acid. *J. Phys. Chem. A* **2009**, *113*, 7294−7303.
(125) Gerbig, D.; Schreiner, P. R. Hydrogen-Tunneling in Biologically Relevant Small Molecules: The Rotamerizations of α-Ketocarboxylic Acids. *J. Phys. Chem. B* **2015**, *119*, 693−703.
(126) Schwabe, T.; Grimme, S. Double-hybrid Density Functionals with Long-range Dispersion Corrections: Higher Accuracy and Extended Applicability. *Phys. Chem. Chem. Phys.* **2007**, *9*, 3397−3406.
(127) Dunning, T. H. Gaussian Basis Sets for Use in Correlated Molecular Calculations. I. The Atoms Boron through Neon and Hydrogen. *J. Chem. Phys.* **1989**, *90*, 1007.
(128) Kendall, A.; Dunning, T. H., Jr.; Harrison, R. J. Electron Affinities of the First-row Atoms Revisited. Systematic Basis Sets and Wave Functions. *J. Chem. Phys.* **1992**, *96*, 6796−6806.
(129) Kozuch, S.; Gruzman, D.; Martin, J. M. L. DSD-BLYP: A General Purpose Double Hybrid Density Functional Including Spin Component Scaling and Dispersion Correction. *J. Phys. Chem. C* **2010**, *114*, 20801−20808.
(130) Frisch, M. J.; Trucks, G. W.; Schlegel, H. B.; Scuseria, G. E.; Robb, M. A.; Cheeseman, J. R.; Scalmani, G.; Barone, V.; Mennucci, B.; Petersson, G. A.; Nakatsuji, H.; Caricato, M.; Li, X.; Hratchian, H. P.; Bloino, J.; Janesko, B. G.; Izmaylov, A. F.; Marenich, A.; Lipparini, F.; Zheng, G.; Sonnenberg, J. L.; Liang, M.; Hada, M.; Ehara, M.; Toyota, K.; Fukuda, R.; Hasegawa, J.; Ishida, M.; Nakajima, T.; Honda, Y.; Kitao, O.; Nakai, H.; Vreven, T.; Throssell, K.; Montgomery, J. A., Jr.; Peralta, J. E.; Ogliaro, F.; Bearpark, M.;

DOI: 10.1021/acs.jctc.5b00580
J. Chem. Theory Comput. XXXX, XXX, XXX−XXX

Heyd, J. J.; Brothers, E.; Kudin, K. N.; Staroverov, V. N.; Keith, T.; Kobayashi, R.; Normand, J.; Raghavachari, K.; Rendell, A.; Burant, J. C.; Iyengar, S. S.; Tomasi, J.; Cossi, M.; Rega, N.; Millam, J. M.; Klene, M.; Knox, J. E.; Cross, J. B.; Bakken, V.; Adamo, C.; Jaramillo, J.; Gomperts, R.; Stratmann, R. E.; Yazyev, O.; Austin, A. J.; Cammi, R.; Pomelli, C.; Ochterski, J. W.; Martin, R. L.; Morokuma, K.; Zakrzewski, V. G.; Voth, G. A.; Salvador, P.; Dannenberg, J. J.; Dapprich, S.; Parandekar, P. V.; Mayhall, N. J.; Daniels, A. D.; Farkas, O.; Foresman, J. B.; Ortiz, J. V.; Cioslowski, J.; Fox, D. J. *Gaussian Development Version, Revision I.03*; Gaussian, Inc.: Wallingford, CT, 2015.

(131) Møller, C.; Plesset, M. S. Note on an Approximation Treatment for Many-Electron Systems. *Phys. Rev.* **1934**, *46*, 618−622.

(132) Woon, D. E.; Dunning, T. H., Jr. Gaussian Basis Sets for Use in Correlated Molecular Calculations. V. Core-valence Basis Sets for Boron through Neon. *J. Chem. Phys.* **1995**, *103*, 4572−4585.

(133) Stanton, J. F.; Gauss, J.; Harding, M. E.; Szalay, P. G. CFOUR A quantum chemical program package. 2011; with contributions from A. A. Auer, R. J. Bartlett, U. Benedikt, C. Berger, D. E. Bernholdt, Y. J. Bomble, O. Christiansen, M. Heckert, O. Heun, C. Huber, T.-C. Jagau, D. Jonsson, J. Jusélius, K. Klein, W. J. Lauderdale, D. Matthews, T. Metzroth, L. A. Mueck, D. P. O'Neill, D. R. Price, E. Prochnow, C. Puzzarini, K. Ruud, F. Schiffmann, W. Schwalbach, S. Stopkowicz, A. Tajti, J. Vázquez, F. Wang, J. D. Watts and the integral packages MOLECULE (J. Almloef and P. R. Taylor), PROPS (P. R. Taylor), ABACUS (T. Helgaker, H. J. Aa. Jensen, P. Jørgensen, and J. Olsen), and ECP routines by A. V. Mitin and C. van Wuellen. For the current version, see http://www.cfour.de (accessed September 13, 2012).

(134) Feller, D. The Use of Systematic Sequences of Wave Functions for Estimating the Complete Basis Set, Full Configuration Interaction Limit in Water. *J. Chem. Phys.* **1993**, *98*, 7059−7071.

(135) Helgaker, T.; Klopper, W.; Koch, H.; Noga, J. Basis-set Convergence of Correlated Calculations on Water. *J. Chem. Phys.* **1997**, *106*, 9639−9646.

(136) Puzzarini, C. Extrapolation to the Complete Basis Set Limit of Structural Parameters: Comparison of Different Approaches. *J. Phys. Chem. A* **2009**, *113*, 14530−14535.

(137) Puzzarini, C.; Barone, V. Extending the Molecular Size in Accurate Quantum-Chemical Calculations: the Equilibrium Structure and Spectroscopic Properties of Uracil. *Phys. Chem. Chem. Phys.* **2011**, *13*, 7189−7197.

(138) Puzzarini, C. Molecular Structure of Thiourea. *J. Phys. Chem. A* **2012**, *116*, 4381−4387.

(139) Truhlar, D. G.; Isaacson, A. D. Simple Perturbation Theory Estimates of Equilibrium Constants from Force Fields. *J. Chem. Phys.* **1991**, *94*, 357−359.

(140) Ayala, P. Y.; Schlegel, H. B. Identification and Treatment of Internal Rotation in Normal Mode Vibrational Analysis. *J. Chem. Phys.* **1998**, *108*, 2314−2325.

(141) Gauss, J.; Stanton, J. F. Analytic CCSD(T) Second Derivatives. *Chem. Phys. Lett.* **1997**, *276*, 70−77.

(142) Puzzarini, C.; Biczysko, M.; Barone, V. Accurate Harmonic/Anharmonic Vibrational Frequencies for Open-Shell Systems: Performances of the B3LYP/N07D Model for Semirigid Free Radicals Benchmarked by CCSD(T) Computations. *J. Chem. Theory Comput.* **2010**, *6*, 828−838.

(143) Puzzarini, C.; Biczysko, M.; Barone, V. Accurate Anharmonic Vibrational Frequencies for Uracil: The Performance of Composite Schemes and Hybrid CC/DFT Model. *J. Chem. Theory Comput.* **2011**, *7*, 3702−3710.

(144) Begue, D.; Carbonniere, P.; Barone, V.; Pouchan, C. Performance of ab initio and DFT/PCM Methods in Calculating Vibrational Spectra in Solution: Formaldehyde in Acetonitrile as a Test Case. *Chem. Phys. Lett.* **2005**, *416*, 206−211.

(145) Begue, D.; Carbonniere, P.; Pouchan, C. Calculations of Vibrational Energy Levels by Using a Hybrid ab Initio and DFT Quartic Force Field: Application to Acetonitrile. *J. Phys. Chem. A* **2005**, *109*, 4611−4616.

(146) Barone, V.; Festa, G.; Grandi, A.; Rega, N.; Sanna, N. Accurate Vibrational Spectra of Large Molecules by Density Functional Computations Beyond the Harmonic Approximation: the Case of Uracil and 2-thiouracil. *Chem. Phys. Lett.* **2004**, *388*, 279−283.

(147) Charmet, A. P.; Stoppa, P.; Tasinato, N.; Giorgianni, S.; Barone, V.; Biczysko, M.; Bloino, J.; Cappelli, C.; Carnimeo, I.; Puzzarini, C. An Integrated Experimental and Quantum-Chemical Investigation on the Vibrational Spectra of Chlorofluoromethane. *J. Chem. Phys.* **2013**, *139*, 164302.

(148) Schuurman, M. S.; Allen, W. D.; von Ragué Schleyer, P.; Schaefer, H. F., III The Highly Anharmonic BH_5 Potential Energy Surface Characterized in the *ab initio* Limit. *J. Chem. Phys.* **2005**, *122*, 104302.

(149) McClurg, R. B.; Flagan, R. C.; Goddard, W. A., III The Hindered Rotor Density-of-States Interpolation Function. *J. Chem. Phys.* **1997**, *106*, 6675−6680.

(150) Zheng, J.; Truhlar, D. G. Including Torsional Anharmonicity in Canonical and Microcanonical Reaction Path Calculations. *J. Chem. Theory Comput.* **2013**, *9*, 2875−2881.

(151) Gordy, W.; Cook, R. L. In *Microwave Molecular Spectra*, 3rd ed.; Weissberger, A., Ed.; Wiley: New York, 1984.

(152) Watson, J. In *Vibrational spectra and structure, Vol.6. A series of advances*; Durig, J., Ed.; Elsevier: Amsterdam, Netherlands, 1977; pp 1−89.

(153) Flygare, W. H. Magnetic Interactions in Molecules and an Analysis of Molecular Electronic Charge Distribution from Magnetic Parameters. *Chem. Rev.* **1974**, *74*, 653−687.

(154) Pawłowski, F.; Jørgensen, P.; Olsen, J.; Hegelund, F.; Helgaker, T.; Gauss, J.; Bak, K. L.; Stanton, J. F. Molecular Equilibrium Structures from Experimental Rotational Constants and Calculated Vibration-Rotation Interaction Constants. *J. Chem. Phys.* **2002**, *116*, 6482−6496.

(155) Piccardo, M.; Penocchio, E.; Puzzarini, C.; Biczysko, M.; Barone, V. Semi-Experimental Equilibrium Structure Determinations by Employing B3LYP/SNSD Anharmonic Force Fields: Validation and Application to Semirigid Organic Molecules. *J. Phys. Chem. A* **2015**, *119*, 2058−2082.

(156) Demaison, J. Experimental, Semi-experimental and Ab Initio Equilibrium Structures. *Mol. Phys.* **2007**, *105*, 3109−3138.

(157) Vogt, N.; Demaison, J.; Ksenafontov, D. N.; Rudolph, H. D. A Benchmark Study of Molecular Structure by Experimental and Theoretical Methods: Equilibrium Structure of Thymine from Microwave Rotational Constants and Coupled-cluster Computations. *J. Mol. Struct.* **2014**, *1076*, 483−489.

(158) Martinez, O.; Crabtree, K. N.; Gottlieb, C. A.; Stanton, J. F.; McCarthy, M. C. An Accurate Molecular Structure of Phenyl, the Simplest Aryl Radical. *Angew. Chem.* **2015**, *127*, 1828−1831.

(159) Puzzarini, C.; Heckert, M.; Gauss, J. The Accuracy of Rotational Constants Predicted by High-level Quantum-Chemical Calculations. I. Molecules Containing First-row Atoms. *J. Chem. Phys.* **2008**, *128*, 194108.

(160) Costain, C. C. Determination of Molecular Structures from Ground State Rotational Constants. *J. Chem. Phys.* **1958**, *29*, 864−874.

(161) Grimme, S.; Antony, J.; Ehrlich, S.; Krieg, H. A Consistent and Accurate ab initio Parametrization of Density Functional Dispersion Correction (DFT-D) for the 94 Elements H-Pu. *J. Chem. Phys.* **2010**, *132*, 154104.

(162) Grimme, S.; Steinmetz, M. Effects of London Dispersion Correction in Density Functional Theory on the Structures of Organic Molecules in the Gas Phase. *Phys. Chem. Chem. Phys.* **2013**, *15*, 16031−16042.

(163) Risthaus, T.; Steinmetz, M.; Grimme, S. Implementation of nuclear gradients of range-separated hybrid density functionals and benchmarking on rotational constants for organic molecules. *J. Comput. Chem.* **2014**, *35*, 1509−1516.

DOI: 10.1021/acs.jctc.5b00580
J. Chem. Theory Comput. XXXX, XXX, XXX−XXX

(164) Schellenberger, A.; Beer, W.; Oehme, G. Untersuchungen zur Theorie der α-ketosäuren-XI. IR-spektroskopische Untersuchungen an αketosäuren im Gaszustand. *Spectrochim. Acta* **1965**, *21*, 1345−1351.
(165) Meyer, R.; Bauder, A. Torsional Coupling in Pyruvic Acid. *J. Mol. Spectrosc.* **1982**, *94*, 136−149.
(166) Puzzarini, C.; Cazzoli, G.; Gauss, J. The Rotational Spectra of $HD^{17}O$ and $D_2{}^{17}O$: Experiment and Quantum-Chemical Calculations. *J. Chem. Phys.* **2012**, *137*, 154311.
(167) Puzzarini, C.; Senent, M. L.; Domínguez-Gómez, R.; Carvajal, M.; Hochlaf, M.; Al-Mogren, M. M. Accurate Spectroscopic Characterization of Ethyl Mercaptan and Dimethyl Sulfide Isotopologues: A Route toward their Astrophysical Detection. *Astrophys. J.* **2014**, *796*, 50.
(168) Marstokk, K.-M.; Møllendal, H. Microwave Spectrum, Conformation, Barrier to Internal Rotation and Dipole Moment of Pyruvic Acid. *J. Mol. Struct.* **1974**, *20*, 257−267.
(169) Biczysko, M.; Latajka, Z. Accuracy of Theoretical Potential Energy Profiles along Proton-Transfer Coordinate for $XH\text{-}NH_3$ (X = F,Cl,Br) Hydrogen-Bonded Complexes. *J. Phys. Chem. A* **2002**, *106*, 3197−3201.
(170) Fornaro, T.; Burini, D.; Biczysko, M.; Barone, V. Hydrogen-Bonding Effects on Infrared Spectra from Anharmonic Computations: Uracil-Water Complexes and Uracil Dimers. *J. Phys. Chem. A* **2015**, *119*, 4224−4236.
(171) Kesharwani, M. K.; Brauer, B.; Martin, J. M. L. Frequency and Zero-Point Vibrational Energy Scale Factors for Double-Hybrid Density Functionals (and Other Selected Methods): Can Anharmonic Force Fields Be Avoided? *J. Phys. Chem. A* **2015**, *119*, 1701−1714.

DOI: 10.1021/acs.jctc.5b00580
J. Chem. Theory Comput. XXXX, XXX, XXX−XXX